AFRL-RW-EG-TR-2014-016

Development of Intake Retention, and Excretion Fractions used in Bioassay Programs for Metallic Nanoparticle Aerosols Produced in Modern Munitions Development

William Godwin
Wesley Bolch

Department of Biomedical Engineering
University of Florida
Gainsville, FL 32611-6131

Charles M. Jenkins

Air Force Research Laboratory
Munitions Directorate/Ordnance Division
Energetic Materials Branch (AFRL/RWME)
Eglin AFB, FL 32542-5910

March 2014

Contract No. FA8651-12-M-0287

Final Report for Period 1 October 2007 – 1 December 2013

AIR FORCE RESEARCH LABORATORY, MUNITIONS DIRECTORATE

Air Force Materiel Command ■ United States Air Force ■ Eglin Air Force Base

NOTICE AND SIGNATURE PAGE

Using Government drawings, specifications, or other data included in this document for any purpose other than Government procurement does not in any way obligate the U.S. Government. The fact that the Government formulated or supplied the drawings, specifications, or other data does not license the holder or any other person or corporation; or convey any rights or permission to manufacture, use, or sell any patented invention that may relate to them.

Qualified requestors may obtain copies of this report from the Defense Technical Information Center (DTIC) (http://www.dtic.mil).

AFRL-RW-EG-TR-2014-016 HAS BEEN REVIEWED AND IS APPROVED FOR PUBLICATION IN ACCORDANCE WITH ASSIGNED DISTRIBUTION STATEMENT.

FOR THE DIRECTOR:

///ORIGINAL SIGNED///	**///ORIGINAL SIGNED///**	**///ORIGINAL SIGNED///**
DAVID E. LAMBERT, PhD Ordnance Sciences Core Technical Competency Lead Ordnance Division	C. MICHAEL LINDSAY, PhD Technical Advisor Energetic Materials Branch	CHARLES M. JENKINS, PhD Project Manager Energetic Materials Branch

This report is published in the interest of scientific and technical information exchange, and its publication does not constitute the Government's approval or disapproval of its ideas or findings.

This page intentionally left blank

REPORT DOCUMENTATION PAGE

Form Approved
OMB No. 0704-0188

1. REPORT DATE *(DD-MM-YYYY)*	**2. REPORT TYPE**	**3. DATES COVERED** *(From - To)*
11-03-2014	Final	01 October 2007 – 01 December 2013

4. TITLE AND SUBTITLE

Development of Intake Retention, and Excretion Fractions used in Bioassay Programs for Metallic Nanoparticle Aerosols Produced in Modern Munitions Development

5a. CONTRACT NUMBER
FA8651-12-M-0287

5b. GRANT NUMBER

5c. PROGRAM ELEMENT NUMBER
62102F

6. AUTHOR(S)

[1]William Godwin, [1]Wesley Bolch, [2]Charles M. Jenkins

5d. PROJECT NUMBER
43479500

5e. TASK NUMBER

5f. WORK UNIT NUMBER
W05R

7. PERFORMING ORGANIZATION NAME(S) AND ADDRESS(ES)

[1]Dept of Biomedical Engineering, University of Florida, Gainesville, FL 32611
[2]Air Force Research Laboratory, AFRL/RWME, Eglin AFB, FL 32542

8. PERFORMING ORGANIZATION REPORT NUMBER

AFRL-RW-EG-TR-2014-016

9. SPONSORING / MONITORING AGENCY NAME(S) AND ADDRESS(ES)

Air Force Research Laboratory, Munitions Directorate
Ordnance Division
Energetic Materials Branch (AFRL/RWME)
Eglin AFB FL 32542-5910
Technical Advisor: C. Michael Lindsay, PhD

10. SPONSOR/MONITOR'S ACRONYM(S)
AFRL-RW-EG

11. SPONSOR/MONITOR'S REPORT NUMBER(S)
AFRL-RW-EG-TR-2014-016

12. DISTRIBUTION / AVAILABILITY STATEMENT

Distribution A: Approved for public release; distribution unlimited. Approval Confirmation 96 ABW/PA #96ABW-2014-4647, dated March 4, 2014

13. SUPPLEMENTARY NOTES **SUBJECT TO EXPORT CONTROL LAWS**
DISTRIBUTION STATEMENT INDICATING AUTHORIZED ACCESS IS ON THE COVER PAGE AND BLOCK 12 OF THIS FORM.
DATA RIGHTS RESTRICTIONS AND AVAILABILITY OF THIS REPORT ARE SHOWN ON THE NOTICE AND SIGNATURE PAGE.

14. ABSTRACT

The current state-of-the-art munitions development by the United States Air Force creates potential exposure scenarios wherein soldiers and laboratory workers may inhale nano-phase aerosols. The primary metals of present interest in this study are aluminum, boron, tantalum, titanium, and tungsten. The contained work describes efforts made to develop a software package capable of analyzing, and predicting, bioassay measurements of workers and soldiers following exposures to the metallic aerosols. The resultant software package (chemIMBA) developed by Dr. Alan Birchall of Public Health England was created by tailoring a pre-existing software package for radioactive aerosol exposures called, Integrated Modules for Bioassay Analysis (IMBA). Biokinetic model selection, and implementation, was conducted for boron, tantalum, titanium, and tungsten. For aluminum, a new systemic biokinetic model was created, and implemented within chemIMBA. Exposures to three different post-detonation blast-aerosols for open air, and enclosed environment scenarios for laboratory workers were simulated using the newly developed chemIMBA software. Intake Excretion Fractions, and Intake Retention Fractions, for time periods up to ten thousand days post-exposure were predicted for exposure scenarios of soldiers and laboratory workers.

15. SUBJECT TERMS
chemIMBA, Inhalation toxicology, Biokinetic models, Excretion rates, Retention equations

16. SECURITY CLASSIFICATION OF:			**17. LIMITATION OF ABSTRACT**	**18. NUMBER OF PAGES**	**19a. NAME OF RESPONSIBLE PERSON**
a. REPORT	**b. ABSTRACT**	**c. THIS PAGE**			Charles M. Jenkins
UNCLASSIFIED	UNCLASSIFIED	UNCLASSIFIED	SAR	62	**19b. TELEPHONE NUMBER** *(include area code)* 850-882-5902

Standard Form 298 (Rev. 8-98)
Prescribed by ANSI Std. Z39.18

This page intentionally left blank

TABLE OF CONTENTS

Section	Title	Page
1.	INTRODUCTION	1
2.	BACKGROUND	2
	A. Potential Toxicological Concerns of Materials of Primary Interest	2
	B. Integrated Modules for Bioassay Analysis	3
	C. IMBA Code Modifications	4
3.	SYSTEMIC BIOKINETIC MODEL FOR TUNGSTEN	5
	A. R.W. Leggett Development of Systemic Tungsten Biokinetic Model	5
	B. IMBA Implementation and Verification of Systemic Tungsten Biokinetic Model	5
4.	IMPLEMENTATION OF A SYSTEMIC BIOKINETIC MODEL FOR ALUMINUM	10
	A. Development of Aluminum Systemic Biokinetic Model	10
	B. Discussion of Aluminum Systemic Biokinetic Model's Predicted Retention In Critical Organs	12
5.	SURROGATE MODEL SELECTION AND IMPLEMENTATION	20
	A. General Considerations for Surrogate Selection	20
	B. Specific Surrogates Selected For chemIMBA Implementation	20
6.	SCENARIOS OF APPLICATION	25
	A. Aerosol Spectra Simulation	25
	B. Battle Field Exposure Scenarios	27
	C. Laboratory Worker Exposure Scenarios	28
	D. Discussion of Exposure Scenario Simulations	29
7.	CONCLUSIONS AND FUTURE WORK	47
	A. Potential Improvements to Fundamentals of chemIMBA Software Package	47
	B. Acquire Element Specific Aerosol Size Distribution Data	47
	C. Refine Biokinetic Models of Elements of Interest	48
	D. The Expansion of Brain Biokinetics to Biokinetic Model of Aluminum	48
	REFERENCES	49
	ACRONYMS	51

LIST OF FIGURES

Figure	Title	Page
1.	Systemic biokinetic model of tungsten	6
2.	Comparison between tungsten retention trends produced by SAAMII software and data points extracted from Figure 6 of Leggett 1997	7
3.	Comparison between tungsten retention trends produced by SAAMII software and biokinetic trends produced by chemIMBA software	8
4.	Recreation of systemic biokinetic model of aluminum	13
5.	All data points extracted from Figure 6 of Steinhausen et al	14
6.	All data points extracted from Figure 7 of Steinhausen et al	15
7.	Newly created systemic biokinetic model for aluminum	16
8.	Comparison of newly created systemic biokinetic model for aluminum predictions of blood retention against bioassay data of two healthy volunteers blood retention	17
9.	Comparison of newly created systemic biokinetic model for aluminum predictions of cumulative urinary excretion against bioassay data of two healthy volunteers cumulative urinary excretion	18
10.	Comparison between biokinetic trends of aluminum produced by SAAMII software and biokinetic trends produced by chemIMBA software	18
11.	Systemic biokinetic model structure developed by ICRP for both zirconium and niobium	21
12.	Comparison between biokinetic trends of titanium produced by SAAMII software and biokinetic trends produced by chemIMBA software	22
13.	Comparison between biokinetic trends of tantalum produced by SAAMII software and biokinetic trends produced by chemIMBA software	22
14.	Biokinetic trends predicted by chemIMBA for a typical battlefield inhalation scenario following a detonation of an explosive containing Blast B formulation	38
15.	Biokinetic trends predicted by chemIMBA for a typical battlefield inhalation scenario following a detonation of an explosive containing Blast C formulation	38
16.	Biokinetic trends predicted by chemIMBA for a typical battlefield inhalation scenario following a detonation of an explosive containing Blast D formulation	39
17.	Biokinetic trends predicted by chemIMBA for a typical laboratory inhalation scenario following a detonation of an explosive containing Blast B formulation	44
18.	Biokinetic trends predicted by chemIMBA for a typical laboratory inhalation scenario following a detonation of an explosive containing Blast C formulation	45

19. Biokinetic trends predicted by chemIMBA for a typical laboratory inhalation scenario following a detonation of an explosive containing Blast D formulation....45
20. ICRP 66 fractional respiratory deposition particle size-dependence compared with representative blast size-distributions....46

LIST OF TABLES

Table Title Page

1. Transfer rates for systemic biokinetic model of tungsten developed by Leggett....9
2. Transfer rates for systemic biokinetic model of aluminum....19
3. Transfer rates for ICRP systemic biokinetic model of niobium for use as tantalum model surrogate....23
4. Transfer rates for ICRP systemic biokinetic model of zirconium for use as titanium model surrogate....24
5. Data-fit parameters produced from Blast B size-distributions....29
6. Data-fit parameters produced from Blast C size-distributions....30
7. Data-fit parameters produced from Blast D size-distributions....30
8. Goodness of fit for Blast B size-distributions....30
9. Goodness of fit for Blast C size-distributions....31
10. Goodness of fit for Blast D size-distributions....31
11. Size-distribution masses and mass-inhalation rates for Blast B....31
12. Size-distribution masses and mass-inhalation rates for Blast C....32
13. Size-distribution masses and mass-inhalation rates for Blast D....32
14. Size-distribution representations for battlefield exposure to Blast B....33
15. Size-distribution representations for battlefield exposure to Blast C....33
16. Size-distribution representations for battlefield exposure to Blast D....33
17. IRF and IEF values for battlefield exposures to Blast B....34
18. IRF and IEF values for battlefield exposures to Blast C....35
19. IRF and IEF values for battlefield exposures to Blast D....36
20. Size-distribution representations for worker exposure to Blast B....39
21. Size-distribution representations for worker exposure to Blast C....39
22. Size-distribution representations for worker exposure to Blast D....40
23. IRF and IEF values for worker exposures to Blast B....40
24. IRF and IEF values for worker exposures to Blast C....41
25. IRF and IEF values for worker exposures to Blast D....43

This page intentionally left blank

1. INTRODUCTION

As a result of the development of high energy dense explosives, the United States Air Force has, as part of the development effort, tested explosives containing nanophase energetic materials. The materials of interest identified in this report are aluminum, tungsten, boron, titanium, and tantalum. Because nanoparticles have been reported in the literature to be capable of entering human cells and causing damage to organelles such as mitochondria and other structures, a need exists for the ability to monitor the exposures of these materials for potential short term and long term effects. Currently, no proactive process of monitoring personnel exposure to particulates exists. This results in having to wait until symptoms are expressed before active intervention to minimize the material exposure can be resolved. The goal of the study is to resolve the issue of monitoring exposures to nanoparticle aerosols and provide a means to reduce and limit the toxicological effects of exposure.

2. BACKGROUND

A. Potential Toxicological Concerns of Materials of Primary Interest

To varying degrees, all metals potentially being implemented in munitions development have associated toxicological concerns. In order to better understand the potentially hazardous effects of the metals, and pin-point anatomical regions that may be of importance in development of comprehensive exposure monitoring capabilities, a review of the most likely implemented elements' toxicology was performed. Primarily, the United States Department of Health toxicological profiles for aluminum and tungsten were investigated.[1, 2]

Regarding aluminum, inhalation exposures are largely not understood. Most associated issues appear to arise simply from the respiratory tract being burdened with inhaled dust, rather than being issues associated with the content of the dust itself. Death due to aluminum inhalation has been observed in workers, as well as for members of the general public. In a case of worker exposures, inhalation of a few years of 51 mg-Al/m^3 (80% Al) dust has been documented as leading to dyspnea, resulting in death. The cause was very likely the aluminum inhaled. This happened to several workers and in one case x-ray images acquired just before death showed signs of pulmonary nodular interstitial fibrosis.[1]

Toxicology associated with other pathways of exposure has been studied more closely. No minimum risk levels have been determined for aluminum, but specific harmful effects of aluminum have been observed in both animals and humans. Delayed maturation, brain issues, decreased weight, and decreased blood cell counts have been found in animal ingestion testing. Dialysis Dementia has been found to be caused by accumulation of aluminum in the brain. Further regarding the brain, there is currently debate as to whether aluminum has a correlation to Alzheimer's disease.[1] It was determined by Priest in 2004 that the exposures of some aluminum workers could result in aluminum body burdens upwards of 800 mg, potentially causing neurological complications.[3] Skeletal effects have been observed in chronic exposure cases. In a number of these cases, skeletal changes have been observed following long term antacid use due to the aluminum content. If enough aluminum is retained in the bone, the bone formation process ceases to properly function, causing AIBD (Aluminium-Induced Bone Disease).[3]

Tungsten inhalation toxicology is not well understood. No cases have been located by the United States Department of Health linking inhalation of tungsten to human death.[2] Most information on tungsten inhalation toxicology comes from toxicology on mixed compounds. Little is known of tungsten inhalation toxicology and its overall long term effect on the human body's processes. Furthermore, potential toxicological effects of tungsten-compounds are often attributed to the presence of cobalt and or chromium which are frequently contained in the compounds in question. Pulmonary fibrosis and the presence of granuloma are the primary issues of concern following inhalation exposure. Some information exists from rodent testing, which claims that tungsten pellets implanted in the muscles of rats can induced aggressive tumor growth in all rat test subjects.[4] These claims were later put in doubt because of the substantial presents of chromium and cobalt in the tungsten alloy. Very little is known about the distribution process of tungsten in humans or its interaction with cellular chemistry. All long-term retention of tungsten is generally assumed to take place in the skeleton. The results of tungsten exposures

are almost entirely extrapolated from animal results. The same follows for tungsten lung deposition.

Based on observations of hard metal workers, tungsten does not appear to be a source of neurological or respiratory complications. Some evidence does exist linking tungsten to potential developmental and reproductive issues in animals and to its influence on co-enzymes of molybdenum.[2]

B. Integrated Modules for Bioassay Analysis

A computational platform does exist for internal radiation exposure bioassay monitoring, namely IMBA (Integrated Modules for Bioassay Analysis).[5] The IMBA software package has been continuously developed since 1997 by The Health Protection Agency (HPA). This software package allows for internal dosimetry monitoring with numerous output and input capabilities; output is both tabular and graphical and allows for data transfer between Windows applications. Since its creation, IMBA has been extensively quality assured, and currently allows for time-dependent bioassay calculations of any user defined organ, or group of organs.[5]

IMBA is a software package originally developed to support International Commission on Radiological Protection (ICRP) requirements to determine the exposure level of human tissues from ingested or inhaled radionuclides. The IMBA software utilizes the research done by the ICRP to create a user friendly computational platform which can be used by mobile laptop computers to monitor radioactive nuclide exposures. Specifically, IMBA makes use of the human respiratory tract model (HRTM) and the human alimentary tract model developed by the ICRP.[5-7]

State-of-the-art respiratory tract particulate exposure monitoring capabilities were incorporated into the model when the ICRP developed the HRTM in its Publication 66. The HRTM resolved several issues of previous models. Notably, the range of relevant particle sizes was expanded greatly. The ICRP Publication 66 model allows for accurate predictions of deposition, clearance, translocation, and excretion of particles and ions from inhaled materials on particle scales down to one half of a nanometer.[6]

For predictions of alimentary tract biokinetics, IMBA employs the ICRP 30 alimentary-tract model. Within the alimentary tract, the anatomical resolution is increased to specifically depict the stomach, small intestine, upper large intestine, and lower large intestine.[7]

In order to model the remaining organs, soft tissue and bones, of the human body, IMBA allows for the addition of user-selected, or user-created, systemic models. The ability to create these models opens up the ability for customization based on specific elements, ages, sexes, or any other variable of interest. Due to the large element dependence of these models, work is continuing to expand the number of available systemic models.

Most IMBA models are comprised of one, or two, central blood compartments: all have rather similar structure with regards to the types of organ compartments and material flow between them. The current systemic model structure being used by the ICRP is intuitive to interpret, leading to vast clinical applicability to additional material models. The over-arching

trend in the past several decades is largely attributed to the switch to recycling models to correct physiological processes which have become identified in recent years.

Recycling models are biokinetic models in which the material of interest does not simply flow from the circulatory system to internal organs and then to excreta, rather, the material of interest is continuously exchanged back-and-forth between physiologically connected compartments via the bloodstream or lymph nodes. The current library of adopted systemic models optimize the competition between computation time and model accuracy. Trying to account for the inaccuracy issues would require increasingly complex models with compartments representing a higher resolution of physiological processes. This would result in an increase in computational time to generate a solution. Based on current requirements, the fundamental model structure appears to be adequate. However, future improvements could be made with the availability of more human data. Several compartment models have been created by Dr. Richard Leggett of Oak Ridge National Laboratory, in large part with the collaboration of the ICRP Committee 2 and its Task Group on Internal Dose (INDOS). Using the methods outlined by Dr. Richard Leggett, future biokinetic models will likely incorporate similar component structure in greater detail if supportive data is available.

C. IMBA Code Modifications

To make use of the IMBA software in monitoring the Air Force exposures, a number of issues had to be addressed concerning deletion of the radioactive decay and the creation of new individual element models. The code needed to be equipped with the ability to interpret mass inputs, rather than IMBA's standard radioactivity input format. Dr. Alan Birchall of the HPA, one of the creators of the IMBA package, was contracted to provide upgrades to the code. Once the necessary changes were made to the software, the final planned addition to IMBA was the implementation of the systemic models for the elements of interest.

The systemic biokinetic models requested by the USAF did not come standard with the original IMBA software package. For implementation in IMBA, full recycling systemic models were created for Al, B, Ti, Ta, and W. A biokinetic tungsten model of standard ICRP format was developed by R. W. Leggett in 1997. This model was chosen for IMBA implementation.[8] This model has been accepted by the ICRP, and was used as the primary model for validation of the methods contained in this work. Further detail on this matter is given in c 3.

The second elemental model of interest was for aluminum. Nolte and Steinhausen developed a model, but this model was found to be lacking and needed modifications in order to grant higher anatomical resolution, in a more anatomically intuitive form.[9, 10] A new aluminum model of familiar ICRP form created in order to properly implement aluminum bioassay monitoring. The details of this model are contained in Section 4. Past development of systemic biokinetic models for the remaining elements of interest, boron, tantalum, and titanium, is limited, and surrogate models were developed based on general trends of elemental biokinetics. More detail regarding these selections is contained in Section 5.

3. SYSTEMIC BIOKINETIC MODEL FOR TUNGSTEN

A. R. W. Leggett Development of Systemic Tungsten Biokinetic Model

In 1997, R. W. Leggett provided a comprehensive review of tungsten research in order to develop a realistic biokinetic model that would provide predictions of elemental concentrations in tissues of exposed populations.[8] The work uses predominantly animal studies to produce a biologically meaningful model with provisional transfer rates. Though earlier tungsten models existed, a requirement was identified for the development of a new model. The primary focus of his work was to create a more biologically realistic model to improve interpretation of currently available exposure data.

Available human data was vastly insufficient for the model development effort. Animal exposures were used as the primary data source for retention times and excretion amounts. Data supporting the development of tungsten's biokinetics was collected from several animal species. When interspecies metabolism differences were observed more importance was given to data regarding dogs, pigs, and goats; animal data gained from rodents, and cows was considered less reliable based on differences between the observed biokinetics of tungsten in these species compared to the biokinetics of tungsten in humans. In order to develop realistic deposition fractions, and ultimately transfer rates, the animal data was used complimentarily with data regarding the biokinetics of molybdenum. Molybdenum, an experimental analogue of tungsten based on their chemical and biological similarities.[8]

The structure of the tungsten biokinetic model, as seen in Figure 1, was borrowed from the model published in ICRP Publication 69 in 1995 for "bone-volume-seeking elements, including uranium."[8] This model was chosen based on similar biokinetic trends between tungsten and the other metals with unpaired electrons in the outer shells. Specifically, comparisons between tungsten and uranium were given as justification for this model structure selection. Both tungsten and uranium show bone as the primary repository for long term retention. Also, the elements show similar physiological pathways, and similar trends of excretion. The model uses first order kinetics to simulate inter-compartmental exchange of tungsten. The numerical descriptor of exchange between compartments was chosen to be 'transfer rates.' The transfer rates are the fraction of compartmental content leaving the source compartment and entering the target compartment per unit time. The transfer rates associated with the tungsten model are reported in units of inverse day, and can be seen in Table 1 of this report.[8]

B. IMBA Implementation and Verification of Systemic Tungsten Biokinetic Model

The model developed by R.W. Leggett was recreated in SAAM II modeling software for future verification of the model's use in chemIMBA. In order to verify the model's correct implementation, results depicted in Figure 6 of Leggett's work were then compared with the model results produced in SAAM II following a single delta-function blood injection exposure simulation for several organs of interest.[8] As shown by Figure 2, the SAAMII recreated model results match well with the data points extracted from Leggett's results.

Dr. Alan Birchall has implemented the Leggett tungsten model into the newly modified chemIMBA software. In order to verify the chemIMBA software's results, retention and

excretion values were compared between the verified SAAMII model and chemIMBA for a single delta-function injection exposure scenario. As shown in Figure 3, with both simulations carried out to ten thousand days post-injection, the resultant compartmental retention matched perfectly between the two software packages. This is an important result in that while both codes employ the same model structure, different mathematical techniques might be employed to solve the system of coupled differential equations needed to make organ and time specific predictions of post-intake material. ChemIMBA is now equipped with the necessary components to predict, and assess bioassay program results for nonradioactive tungsten exposures.

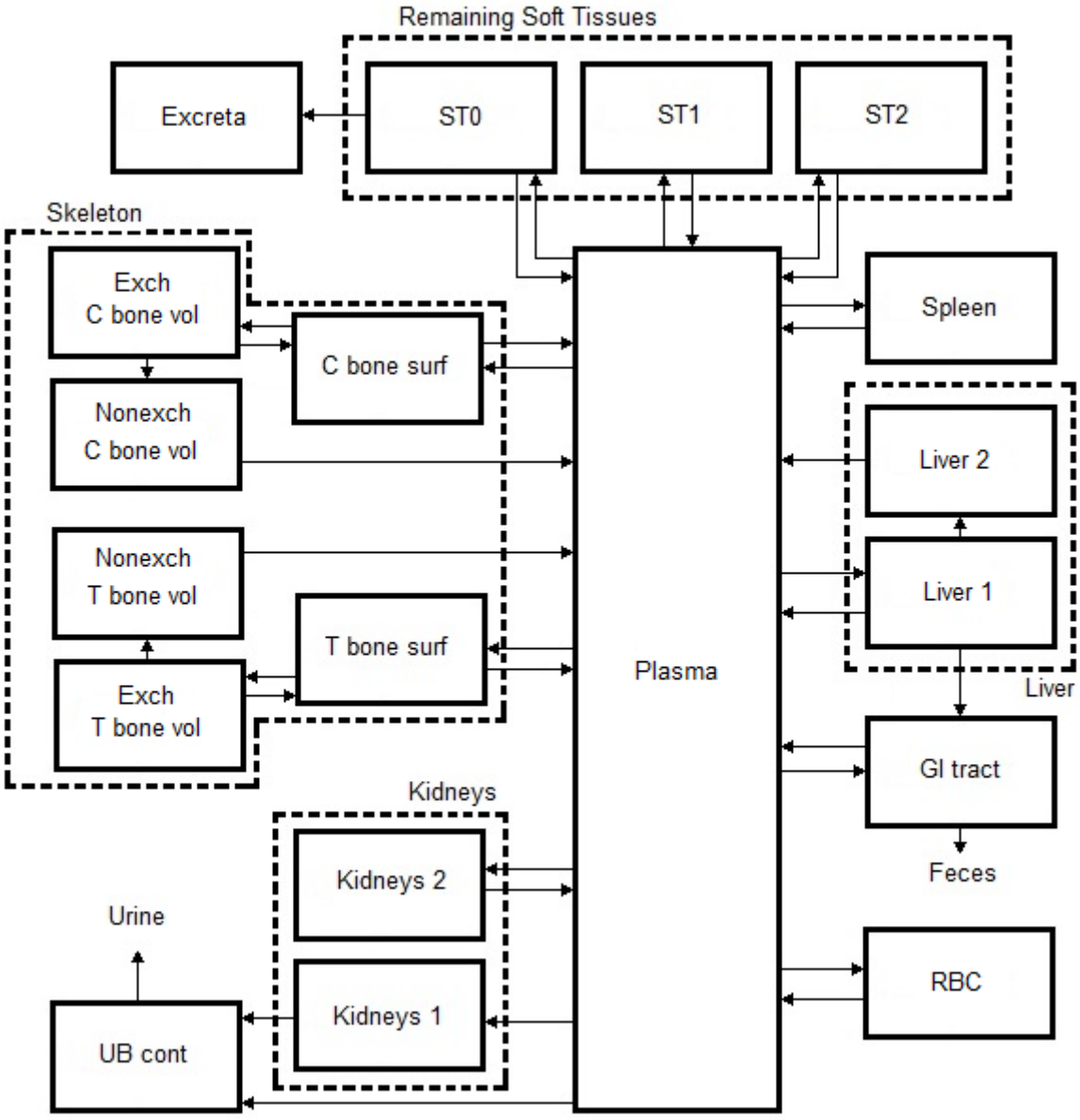

Figure 1. Systemic biokinetic model of tungsten implemented in chemIMBA. Recreated from model developed by Leggett.[8]

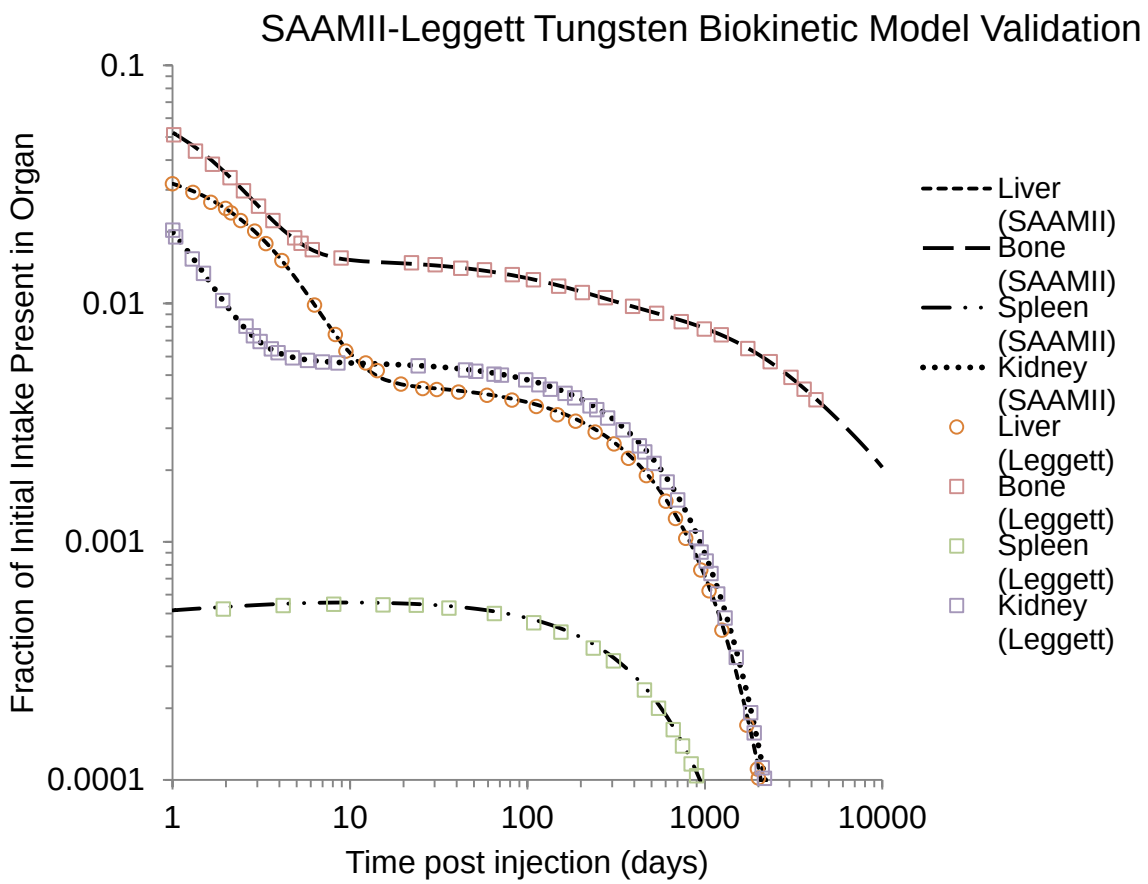

Figure 2. Comparison between tungsten retention trends produced by SAAMII software and data points extracted from figure 6 of Leggett 1997.[8] Used for verification of tungsten model recreation in SAAMII.

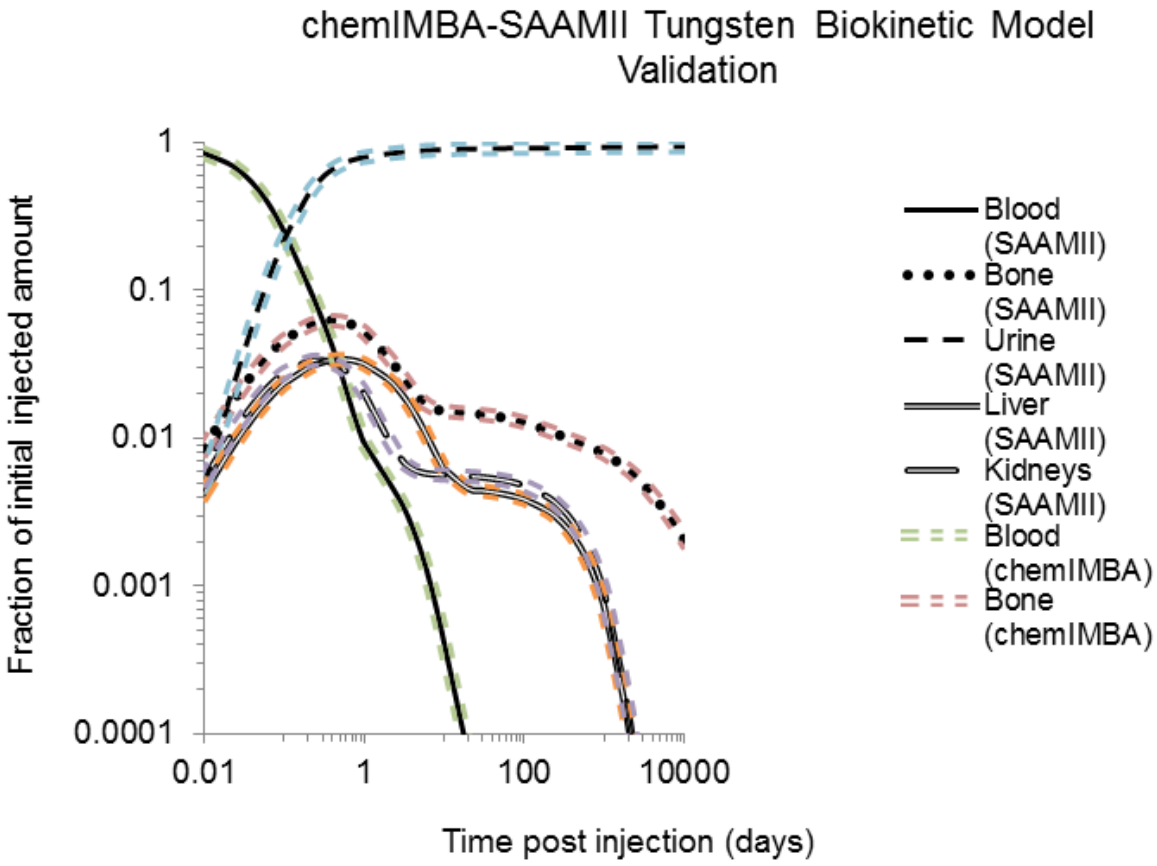

Figure 3. Comparison between biokinetic trends of tungsten produced by SAAMII software and biokinetic trends produced by chemIMBA software.

Table 1. Transfer rates for systemic biokinetic model of tungsten developed by Leggett[8]

From	To	Transfer Rate [day^{-1}]
Plasma	ST0	4.99E+00
Plasma	RBC	5.82E-02
Plasma	UB cont	8.74E+00
Plasma	Kidneys 1	5.24E-01
Plasma	Kidneys 2	5.82E-02
Plasma	ULI cont	5.82E-01
Plasma	Spleen	5.82E-03
Plasma	Liver 1	4.66E-01
Plasma	ST1	2.62E-01
Plasma	ST2	2.33E-02
Plasma	T bone surf	5.18E-01
Plasma	C bone surf	4.14E-01
ST0	Plasma	8.32E+00
RBC	Plasma	3.47E-01
Kidneys 1	UB cont	1.39E+00
Kidneys 2	Plasma	1.90E-03
Liver 1	Plasma	3.12E-01
Liver 1	Liver 2	3.47E-02
ST1	Plasma	6.93E-02
ST2	Excreta	1.90E-03
Spleen	Plasma	1.90E-03
T bone surf	Plasma	5.78E-01
T bone surf	Exch T bone vol	1.16E-01
C bone surf	Plasma	5.78E-01
C bone surf	Exch C bone vol	1.16E-01
Liver 2	Plasma	1.90E-03
Nonexch T bone	Plasma	4.93E-04
Nonexch C bone	Plasma	8.21E-05
Exch T bone vol	T bone surf	2.77E-03
Exch T bone vol	Nonexch T bone vol	4.16E-03
Exch C bone vol	C bone surf	2.77E-03
Exch C bone vol	Nonexch C bone vol	4.16E-03

Transfer rates are associated with the model structure seen in Figure 1.

4. IMPLEMENTATION OF A SYSTEMIC BIOKINETIC MODEL FOR ALUMINUM

A. Development of Aluminum Systemic Biokinetic Model

The current state of aluminum systemic biokinetic modeling is one of continuing improvement. Biokinetic models do exist with urinary excretion and blood retention predictions validated by human testing.[9, 10] However, the previously developed models largely depict the kinetics of aluminum in a physiochemical framework rather than within an ICRP-like anatomical framework. In order to create a more anatomically intuitive systemic model structure for aluminum biokinetics, a comprehensive literature search was completed. Pertinent work produced by Taylor, Leggett, Steinhausen, Nolte, and Priest was acquired. Ultimately, kinetics related to blood retention and urinary excretion were developed by being empirically fit based on adult male injection data acquired by Steinhausen et al.[10] Bone retention was addressed by fundamental physiological considerations of bone remodeling rates in adults. The matching of current model predictions to that of bone retention trends generated by Nolte and Steinhausen were then compared.[3, 9-11] Liver and spleen retention was determined based on the conclusions of Nolte et al. which predicted rapid uptake of aluminum, but no long-term retention.[9]

In 2004, Steinhausen et al. advanced aluminum biokinetics by conducting a study of six healthy volunteers and two patients with chronic renal failure. All test subjects were administered ^{26}Al as a tracer and accelerator mass spectroscopy was performed to determine the biokinetic trends of the aluminum. Following delta-function administration of aluminum, orally in some cases and intravenously in others, urine and blood activity bioassay were completed periodically. The bioassay data was then compared to the predictions created by a systemic biokinetic model, whose structure was developed by Nolte et al. and can be seen in Figure 4. From these values, the appropriate time constants were derived for retention, deposition, and excretion.[9, 10] The model generates predictions of retention for numerous organs including bone, muscle, and blood. However, the level of anatomical resolution given to bone retention was limited. Furthermore, the biokinetics of aluminum in blood was broken down further than the level necessary for anatomical clarity; circulatory aluminum was compartmentalized based on chemical binding of aluminum in the body.

The development of the new systemic model was motivated by the desire to create a potential increase in anatomical resolution of biokinetics relating to bone, liver, spleen, and kidneys. Secondarily, the newly developed model aimed to reduce aluminum biokinetic dependence on the chemical division of circulatory aluminum's compartmentalization; circulatory aluminum representation was reduced to a single compartment rather than four compartments as proposed by Nolte et al.[9] Initially, the Leggett tungsten biokinetic model structure was used as the base structure for development of the new aluminum model.[8] This model structure was employed due to the fact that bone sites tend to be the long-term repository for both aluminum and tungsten.[3, 8]

Data points from the work done by Steinhausen were extracted and used to fit modeling parameters; data points from Figures 6 and 7 of Steinhausen were extracted for urine, plasma, bone, and organs. All Steinhausen data points used for aluminum trend fitting can be seen in Figure 5 and Figure 6 of this report.[10] The urinary excretion and blood retention data collected following intravenous administration of aluminum in two healthy subjects by Steinhausen were

used to empirically fit biokinetic model transfer rates related to blood retention and urinary excretion. The results of the Nolte et al. model predictions for bone, liver, and spleen retention of the two healthy patients were used to assist in iteratively perfecting transfer rates between anatomical compartments. Notably, during the process of fitting all model transfer rates, the data collected via human urinary excretion and blood retention sampling were always given precedent over previous model organ content estimates.

Using the Leggett tungsten structure and the data extracted from Steinhausen et al., SAAMII software was used in order to iteratively produce transfer rates between compartments. Repeatedly, fits that followed retention trends well did not generate physiologically relevant transfer rates; transfer rates generated by fits implied biokinetics with unreasonably high, and low, rates of exchange between compartments. Physiological considerations were then set in place for all transfer rates in order to allow the fitting process to be limited by numerical bounds that had potential physiological explanations.

The bounds of the fit-generated transfer rates related to bone uptake were adjusted based on consideration of trends observed in biokinetics of elements that tend to use bone as a long term repository. The resultant inference is that the rate of removal from deep bone volume is independent of the element of interest and is solely controlled by the rate of bone remodeling and turnover. [8, 12] Thus, transfer rates from deep bone volume to compartments associated with circulatory retention were locked at constant values and not allowed to be changed during the fitting process.

Bounds for remaining transfer rates between compartments were established by compiling a reference list of rates used for various elemental biokinetic models with similar systemic structure. The list of transfer rates were compiled by various works conducted by Leggett et al. and D.M. Taylor, and included rates for tungsten, cesium, cobalt, manganese, ruthenium, and all lanthanide elements.[8, 12-16] All transfer rates between compartments of the aluminum model were given lower bounds correlating to the lowest valued transfer rate of all elements contained in the compiled reference list. Upper bounds were assigned based on the highest valued transfer rate of all elements contained in the compiled reference list.

With the newly selected bounds used when fitting the transfer rates, the model no longer was capable of predicting retention and excretion trends that were agreeable with available human data. While efforts were continued to fit the data using the tungsten structure, the literature search was resumed to explore other avenues of developing a solution.

The conclusion of a comprehensive summary of aluminum biokinetics done by N.D. Priest in 2004 led to a key adjustment in the development of the aluminum biokinetic model presented in this work.[3] Priest concluded that the biokinetics of aluminum follow similar trends as other trivalent metals. Of specific importance to this work, Priest made the assertion that aluminum's biokinetics should be similar to that of the lanthanide elements.[3] This conclusion guided the modeling of this project in the correct direction of using a lanthanide systemic model structure as developed by D.M. Taylor and R.W. Leggett.[11] The model structure for the in-progress aluminum model was then changed to mimic the known structure of the lanthanide biokinetic model. The model structure for aluminum was now identical to that of the

lanthanides, with the addition of a model compartment representing the exchange of material between blood and the spleen. The transfer rates for all lanthanides were used as an approximation for the order of magnitude of aluminum's transfer rates and appropriate bounds for transfer rate fitting were chosen. Attempts were made to follow trends predicted by the ionic-radius dependence of lanthanide transfer rates noted by Taylor and Leggett.[12] However, when fitting the known human data for aluminum and attempting to follow the ionic-radius trends, a reliable fit could not be established. As a result, the transfer rates restricted by this trend were given more freedom during the fitting process. The Steinhausen data was then fit to the new aluminum model structure. Preliminary transfer rates were produced by the SAAMII software package fitting process.

After several iterations of model fitting, final values of transfer rates were established. The finalized transfer rates, as seen in Table 2, were applied to the new aluminum model structure as shown in Figure 7. Comparisons between model predictions following a delta-function intravenous injection scenario and human blood retention, and urinary excretion data gathered by Steinhausen et al., can be seen in Figure 8 and Figure 9, respectively.[10] For verification of the model's results, the finalized systemic biokinetic model was used to simulate a delta-function injection scenario in both SAAM II and chemIMBA packages. The two packages created identical results; the model predictions of retention in several critical organs, and urinary excretion, can be seen in Figure 10.

B. Discussion of Aluminum Systemic Biokinetic Model's Predicted Retention In Critical Organs

The predictions of the current model's long-term retention of aluminum matched the results of previous biokinetic modeling results well; bone retention is vastly the primary site of long term aluminum retention.[10] The systemic aluminum is expected to largely be bound to the bone by organic bone matrix processes. The bone binding process eventually leads to aluminum being deeply bound within the bone after the bone grows over the aluminum contaminated surfaces. Such long-term bound aluminum's rate of exchange is almost exclusively controlled by the element-independent rate of bone growth and resorption.[3] Furthermore, the aluminum retention in the liver and spleen simulated by the newly created model predicts that the liver and spleen appear to collect a large fraction of systemic aluminum in earlier time scales post exposure, but quickly lose their acquired aluminum. This trend was predicted in past biokinetic model work by Nolte et. al. based on retention trends observed in rodents.[9] This trend was also predicted by Priest in his analysis of aluminum in comparison to trends of trivalent metals.[3] The retention of aluminum within the kidneys follows a similar trend as that of the liver and spleen. This result was generated largely by the consideration of two primary issues. The kidney retention was directly dependent on the trends of urinary excretion. In healthy test subjects data regarding the relative retention of the liver and spleen cumulatively, in comparison to kidneys, has largely been inconclusive.[3] Thus, transfer rates associated with the kidneys were chosen with the goal of producing similar retention trends as that of all soft tissues while still allowing for correct urinary excretion predictions.

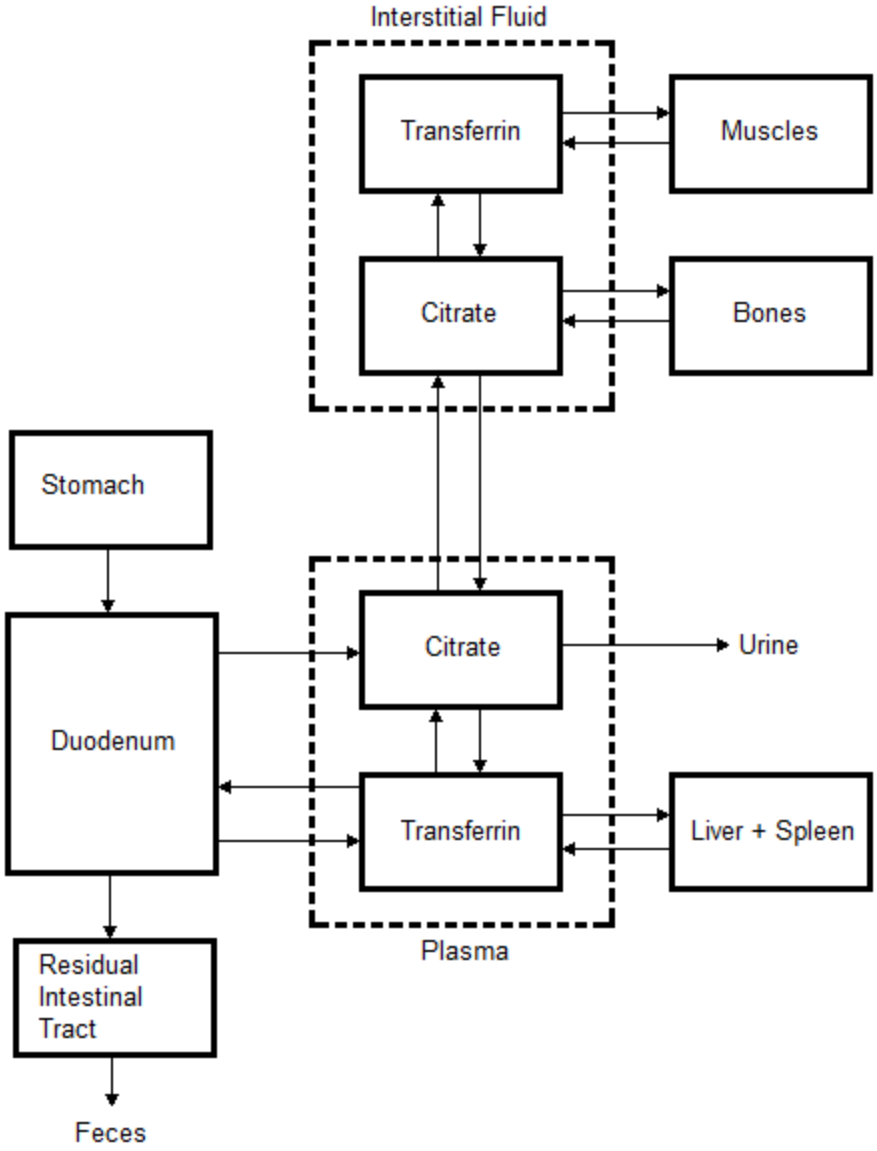

Figure 4. Recreation of systemic biokinetic model of aluminum as developed Nolte et al.[9]

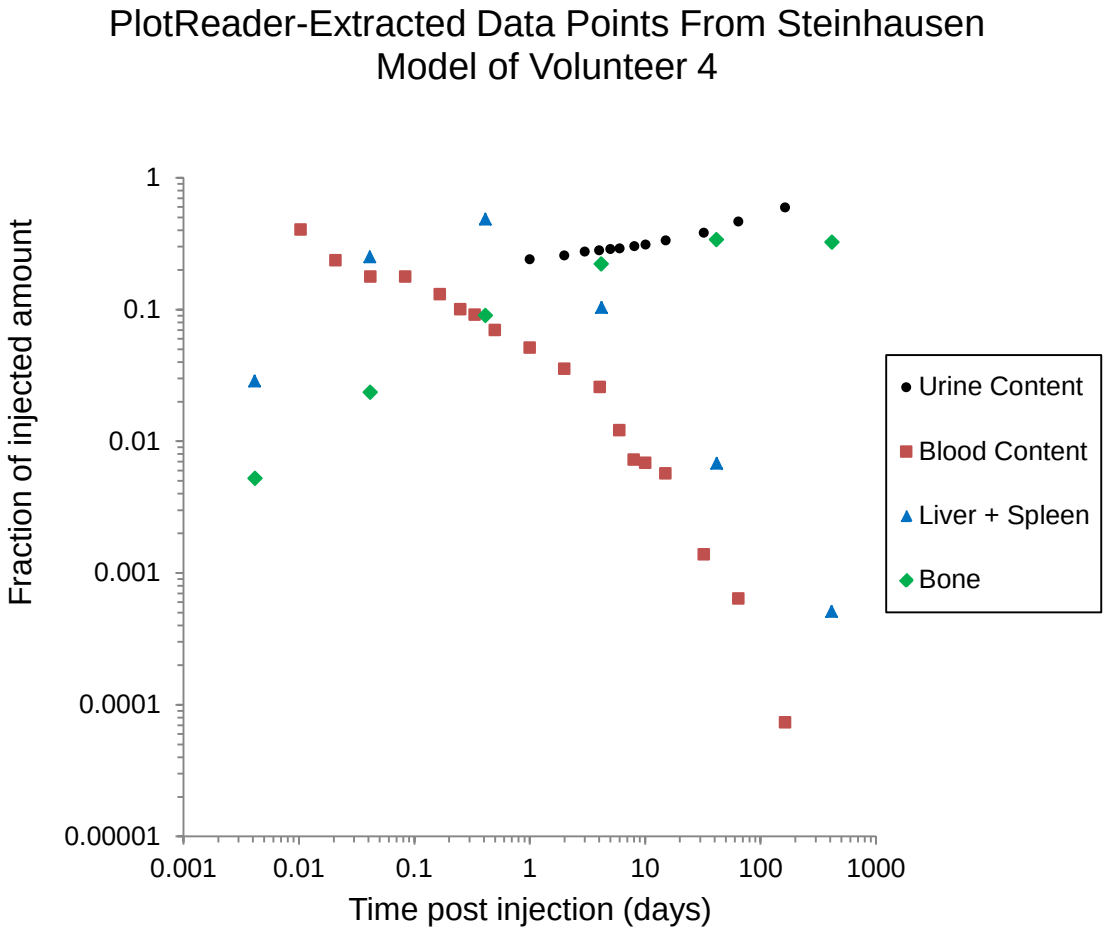

Figure 5. All data points extracted from Figure 6 of Steinhausen et al. for use in transfer rate determination of newly created biokinetic model of aluminum. Blood and Urine data points are actual physical bioassay measurements of healthy volunteer 4.[10]

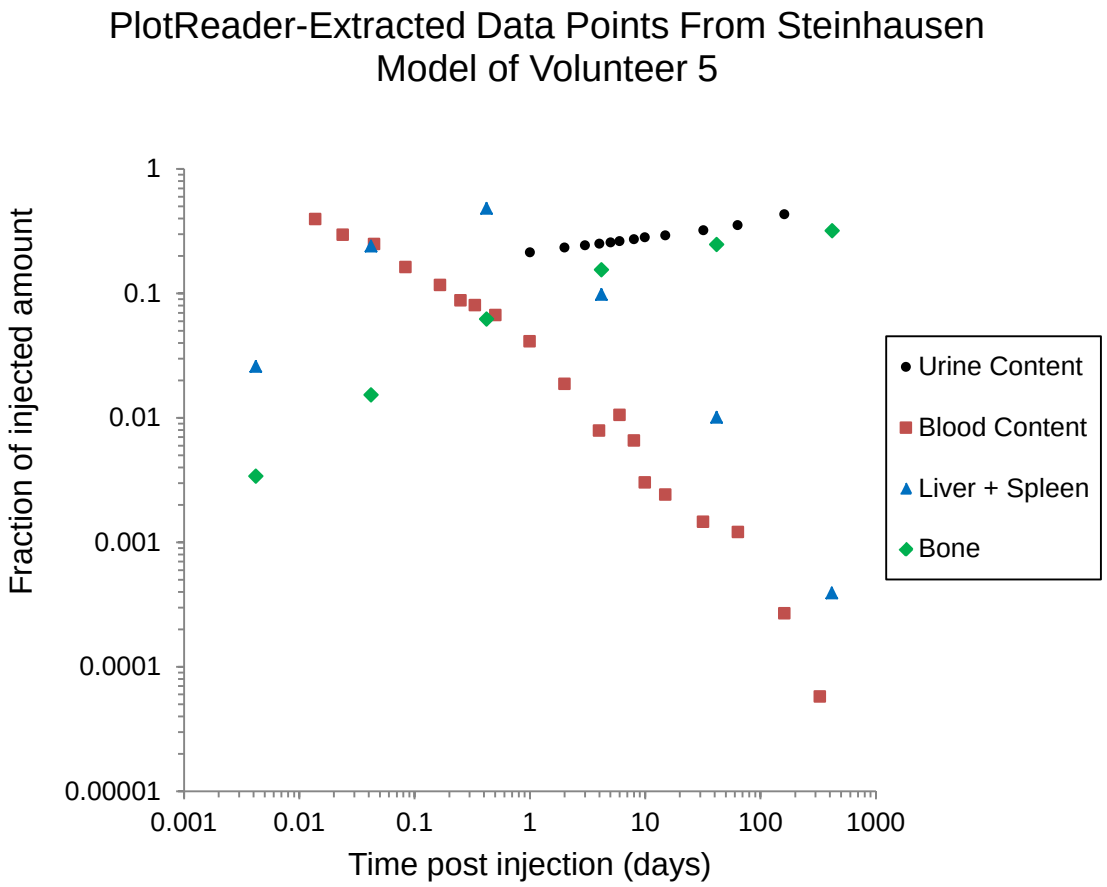

Figure 6. All data points extracted from Figure 7 of Steinhausen et al. for use in transfer rate determination of newly created biokinetic model of aluminum. Blood and Urine data points are actual physical bioassay measurements of healthy volunteer 5.[10]

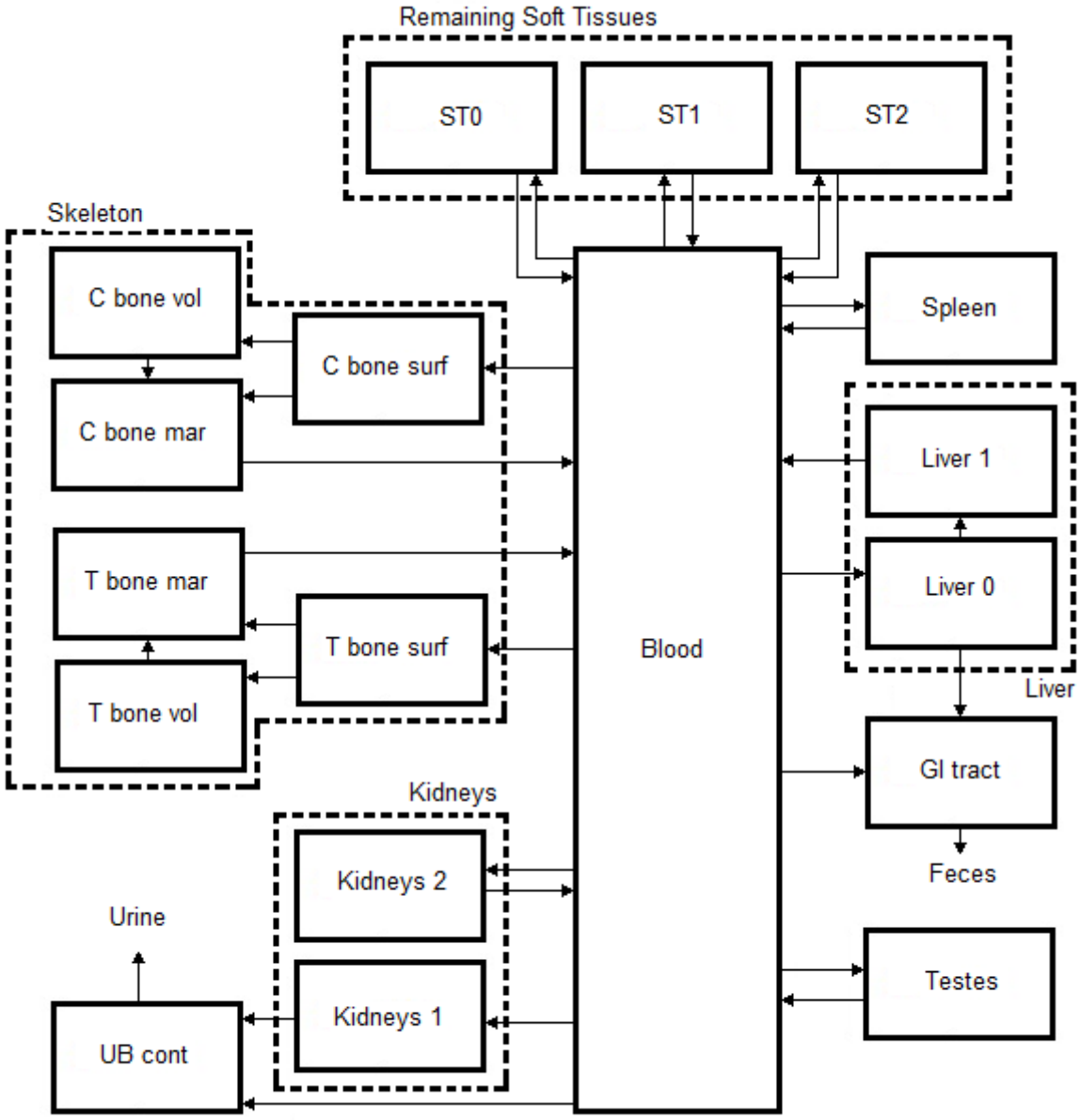

Figure 7. Newly created systemic biokinetic model for aluminum, implemented by chemIMBA

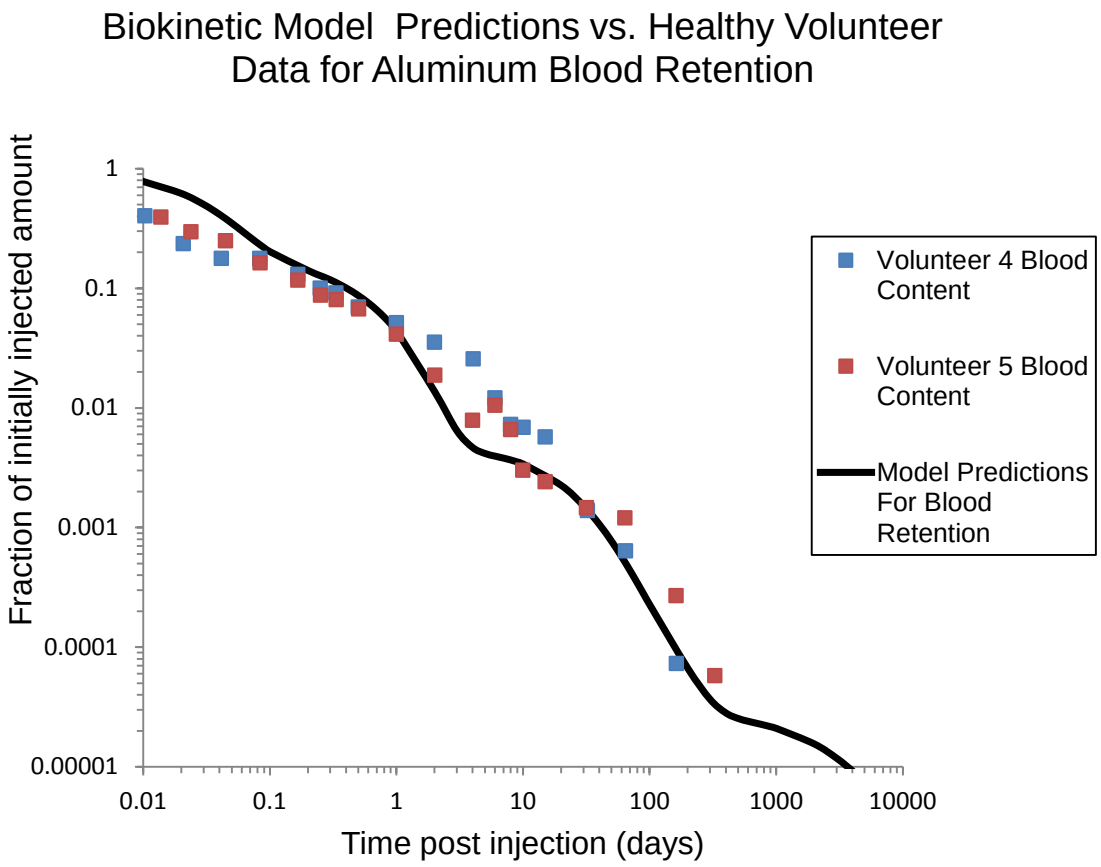

Figure 8. Comparison of newly created systemic biokinetic model for aluminum predictions of blood retention against bioassay data of two healthy volunteers blood retention acquired by Steinhausen et al[10]

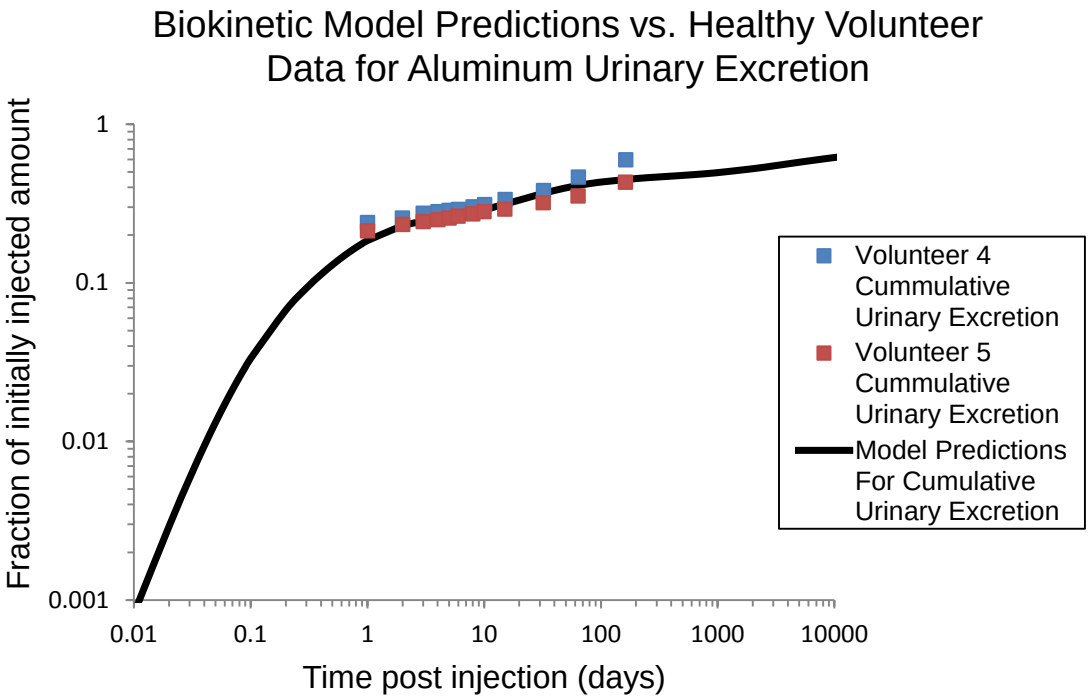

Figure 9. Comparison of newly created systemic biokinetic model for aluminum predictions of cumulative urinary excretion against bioassay data of two healthy volunteers cumulative urinary excretion acquired by Steinhausen et al[10]

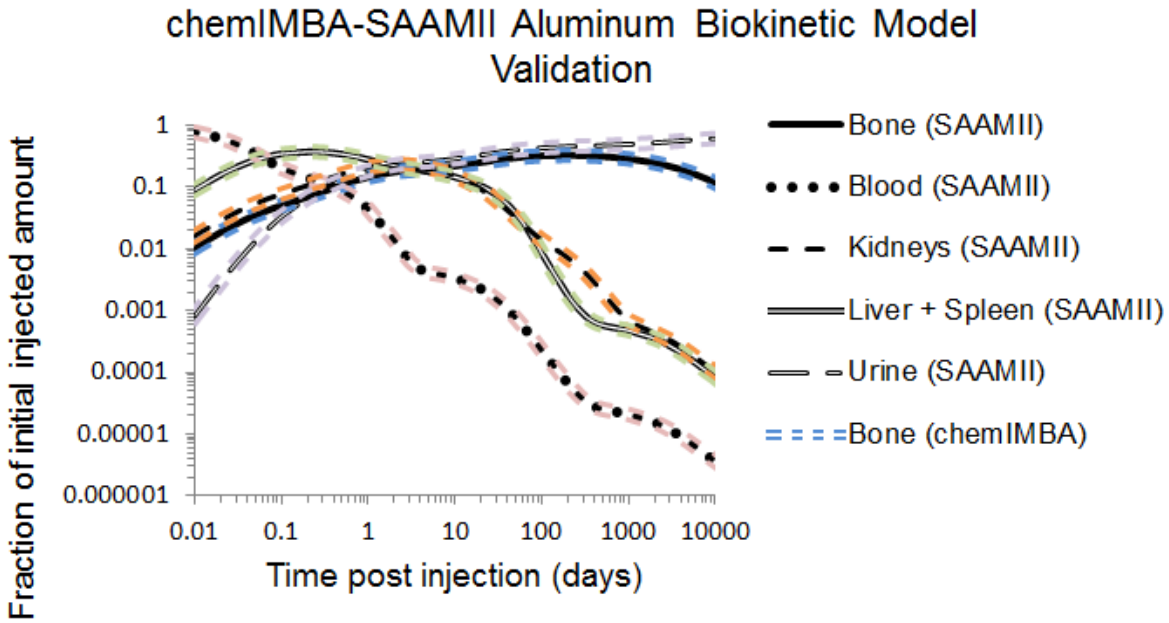

Figure 10. Comparison between biokinetic trends of aluminum produced by SAAMII software and biokinetic trends produced by chemIMBA software

Table 2. Transfer rates for systemic biokinetic model of aluminum

From	To	Transfer Rate [day^{-1}]
Blood	Liver 0	1.500E+00
Blood	ST0	9.937E+00
Blood	ST1	4.097E-01
Blood	ST2	4.323E-05
Blood	C bone surf	5.900E-01
Blood	T bone surf	5.900E-01
Blood	Kidneys 1	5.000E-02
Blood	ULI cont	1.100E-01
Blood	Kidneys 2	1.776E+00
Blood	Testes	6.000E-03
Blood	UB cont	1.546E+00
Blood	Spleen	9.000E+00
Liver 1	Blood	5.860E-02
Liver 0	SI cont	1.123E-01
Liver 0	Liver 1	1.800E-01
ST0	Blood	1.000E+01
ST1	Blood	1.500E-02
ST2	Blood	5.000E-03
C bone mar	Blood	2.040E-02
C bone surf	C bone mar	8.210E-05
C bone surf	C bone vol	5.000E-06
C bone vol	C bone mar	8.210E-05
T bone mar	Blood	2.040E-02
T bone surf	T bone mar	4.930E-04
T bone surf	T bone vol	2.000E-03
T bone vol	T bone mar	4.930E-04
Kidneys 1	UB cont	5.000E-03
Kidneys 2	Blood	1.006E-01
Testes	Blood	3.800E-04
Spleen	Blood	5.000E+00
UB cont	Urine	1.200E+01
GI	Feces	1.000E+00

Transfer rates are associated with the model structure seen in Figure 7.

5. SURROGATE MODEL SELECTION AND IMPLEMENTATION

A. General Considerations for Surrogate Selection

With the successful implementation of both tungsten and aluminum models, three elements remained for necessary chemIMBA implementation. If research regarding the biokinetics of a certain element were determined to be too sparse or too inconclusive to lead to development of a physiologically meaningful biokinetic model, a preliminary surrogate model was selected. Boron, tantalum, and titanium were determined to require model surrogates. Selection of this surrogate is meant to give the best available approximation for the biokinetics of the element of interest. Furthermore, if future data regarding the biokinetics of the element of interest were to be collected, these surrogates present a model structure that may provide a useful setting for interpretation of data and future model development.

Surrogates were chosen on the basis of both chemical and physical similarity to the element of interest. When searching for a surrogate systemic model, three primary issues were considered: the surrogate must be within the same elemental group as the element of interest; the atomic mass of the two elements must be as close as possible within their elemental group; the biokinetic model for the surrogate element should be as extensively tested as possible, with human data validation if available. Following these guidelines, surrogate models were selected to represent boron, tantalum, and titanium.

B. Specific Surrogates Selected For chemIMBA Implementation

The preliminary niobium and zirconium models, developed by the ICRP for occupational intakes of radionuclides, were used as surrogates for tantalum and titanium, respectively. These models share a model structure, but have different associated transfer rates in order to represent their varying biokinetic trends. Notably, niobium tends to exchange from blood to bone more slowly than zirconium, and has a greater deposition in soft tissues. Furthermore, niobium exhibits a higher rate of urinary excretion than that of zirconium. The model structure for both elements can be seen in Figure 11, and the associated transfer rates for niobium and zirconium can be seen in Table 3, and Table 4, respectively.

Following the models' additions to the chemIMBA library, verification of the chemIMBA simulation's results were determined by comparison with SAAMII model results for a single delta-function injection exposure scenario. As can be seen for tantalum and titanium, respectively in Figure 12 and Figure 13, with both simulations carried out to ten thousand days post-injection, the resultant compartmental retention and excretion matched perfectly between the two software packages. With the integration of the verified niobium and zirconium model, chemIMBA was made capable of predicting, and assessing, bioassay program results for nonradioactive tantalum and titanium exposures.

The aluminum model developed previously in this work is being used as the surrogate for boron biokinetics. Development, implementation, and verification of this model are described in Section 4 of this work.

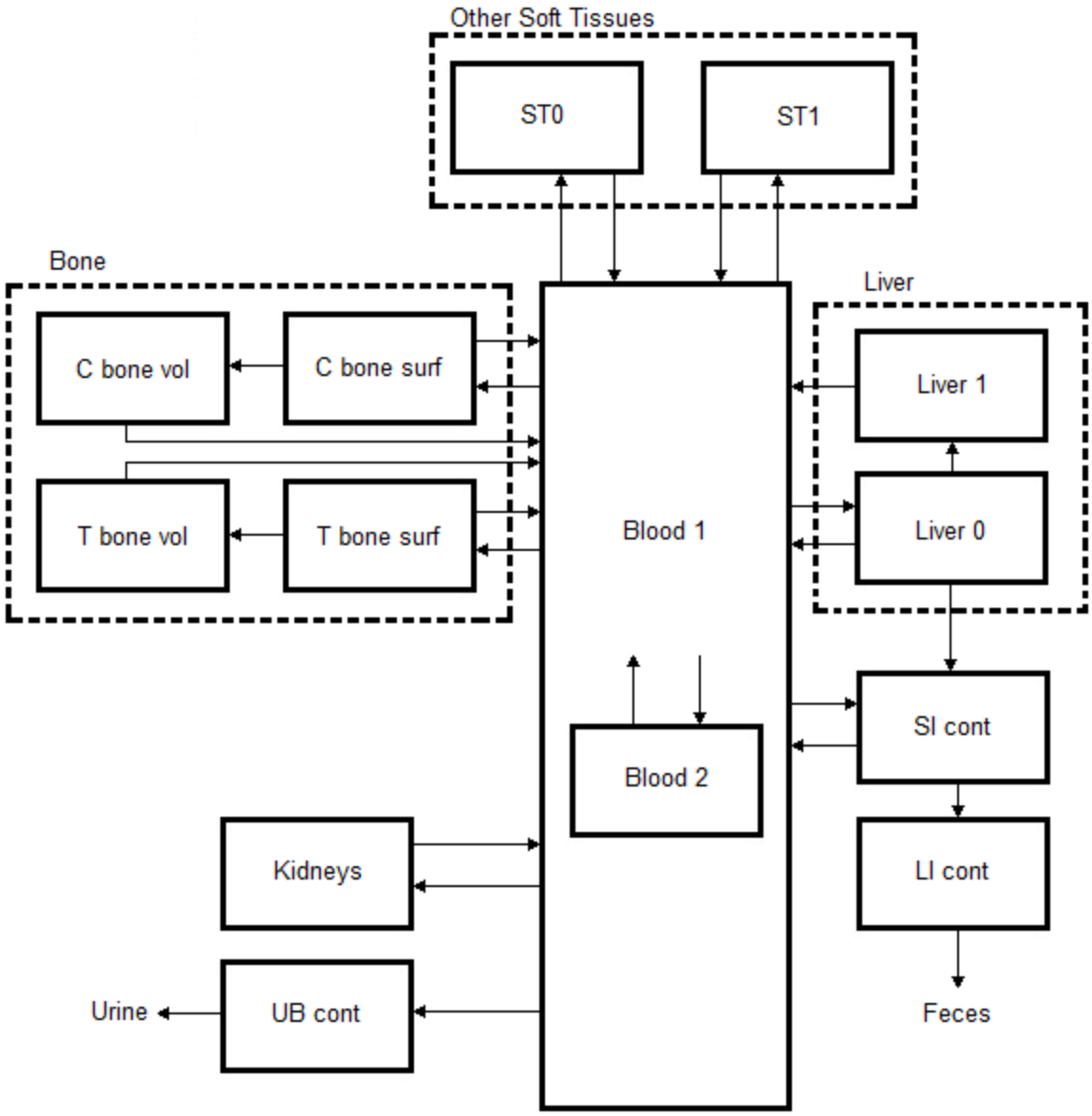

Figure 11. Systemic biokinetic model structure developed by ICRP for both zirconium and niobium, and implemented as a surrogate for both tantalum and titanium

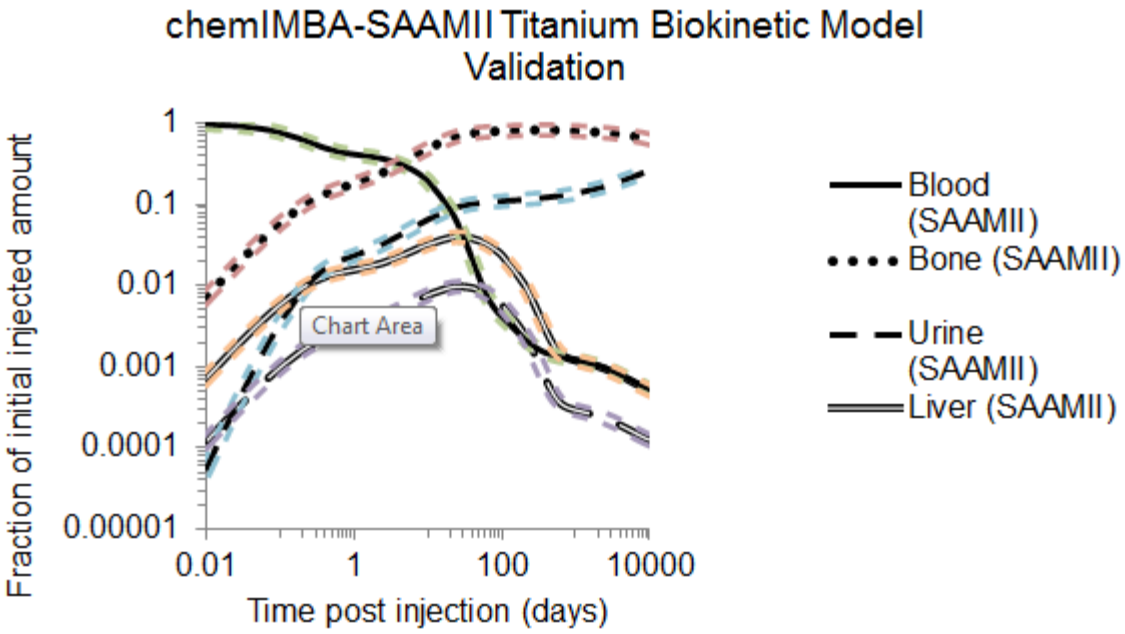

Figure 12. Comparison between biokinetic trends of titanium produced by SAAMII software and biokinetic trends produced by chemIMBA software

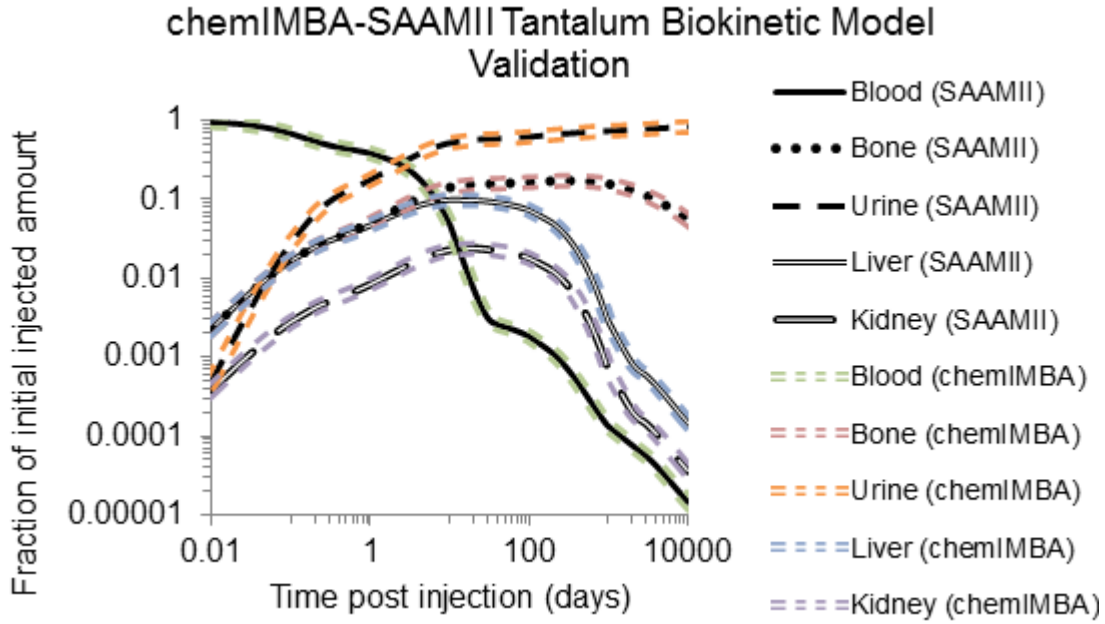

Figure 13. Comparison between biokinetic trends of tantalum produced by SAAMII software and biokinetic trends produced by chemIMBA software

Table 3. Transfer rates for ICRP systemic biokinetic model of niobium for use as tantalum model surrogate

From	To	Transfer Rate [day^{-1}]
Blood 1	Blood 2	3.2000E+00
Blood 1	Liver 0	2.4000E-01
Blood 1	Kidneys	4.0000E-02
Blood 1	ST0	3.2000E+00
Blood 1	ST1	1.2000E-01
Blood 1	UB cont	8.8000E-01
Blood 1	SI cont	8.0000E-02
Blood 1	T bone surf	1.2000E-01
Blood 1	C bone surf	1.2000E-01
Blood 2	Blood 1	1.3900E+00
Liver 0	SI cont	5.7800E-02
Liver 0	Blood 1	5.7800E-02
Liver 0	Liver 1	2.3100E-01
Liver 1	Blood 1	5.0000E-03
Kidneys	Blood 1	5.0000E-03
ST0	Blood 1	1.3900E+00
ST1	Blood 1	1.0000E-02
T bone surf	Blood 1	4.9300E-04
T bone surf	T bone vol	2.4700E-04
T bone vol	Blood 1	4.9300E-04
C bone surf	Blood 1	8.2100E-05
C bone surf	C bone vol	4.1100E-05
C bone vol	Blood 1	8.2100E-05

Transfer rates are associated with the model structure seen in Figure 11

Table 4. Transfer rates for ICRP systemic biokinetic model of zirconium for use as titanium model surrogate

From	To	Transfer Rate [day^{-1}]
Blood 1	Blood 2	2.0000E+00
Blood 1	Liver 0	7.5000E-02
Blood 1	Kidneys	1.2500E-02
Blood 1	ST0	2.0000E+00
Blood 1	ST1	3.7500E-02
Blood 1	UB cont	1.0000E-01
Blood 1	SI cont	2.5000E-02
Blood 1	T bone surf	3.7500E-01
Blood 1	C bone surf	3.7500E-01
Blood 2	Blood 1	4.6200E-01
Liver 0	SI cont	1.1600E-01
Liver 0	Blood 1	1.1600E-01
Liver 0	Liver 1	4.6200E-01
Liver 1	Blood 1	1.0000E-02
Kidneys	Blood 1	1.0000E-02
ST0	Blood 1	4.6200E-01
ST1	Blood 1	2.0000E-02
T bone surf	Blood 1	4.9300E-04
T bone surf	T bone vol	2.4700E-04
T bone vol	Blood 1	4.9300E-04
C bone surf	Blood 1	8.2100E-05
C bone surf	C bone vol	4.1100E-05
C bone vol	Blood 1	8.2100E-05

Transfer rates are associated with the model structure seen in Figure 11

6. SCENARIOS OF APPLICATION

A. Aerosol Spectra Simulation

In order to simulate an aerosol particle distribution, IMBA software requires lognormal parameter inputs and information on the given materials absorption and shape characteristics. It is assumed that aluminum's fractional absorption (f_1) follows similar trends to that of all lanthanide elements and was selected to have a value of 0.0005.[17] At the recommendation of ICRP 66, the aluminum aerosol of interest was classified as a "type F" material, representative of a high rate of dissolution appropriate for gases and vapors.[6] In the event of an inhalation exposure, the parameters used by chemIMBA to describe the particle size-distribution are inputs of single lognormal distribution parameters, count median particle diameter (CMD) and the associated geometric standard deviation. Though the physical reason has not yet been discovered, most single source aerosols size distributions are very well represented by the lognormal distribution. Thus, it is the standard manner of simulating aerosol spectra.[18]

In 2004, Cheng and Jenkins performed work to study the types of distributions that may be produced by our explosives of interest.[19] It was found that the population of workers and soldiers coming into contact with the nanoparticles are not simply interacting with monodisperse particle distributions, nor are they always coming into contact with polydisperse particle distributions that can be reasonably approximated by a single lognormal distribution; many of the aerosols of interest are polymodal particle distributions generated by an explosive charge upon detonation.

Cheng and Jenkins undertook measurements of two aluminum nanophase powder formulations, and one micron aluminum powder formulation. The formulation containing 1.5 μm diameter aluminum powder is nominally referred to as Blast B. The nanophase formulations containing 100 nanometer diameter aluminum powder and 50 nanometer diameter aluminum powder were referred to as Blast C and Blast D, respectively. After detonation, all three formulations produced polydisperse distributions ranging from tens of nanometers up to several hundred nanometers. The particle size distributions for each of the blasts were measured over a period of several minutes post-detonation at regular intervals; the particle distributions were measured in intervals of one minute or one and a half minutes. Comprehensive particle distribution time-dependence was determined. The data presented was in the form of the normalized particle number concentration versus particle diameter.[19] In order to utilize this data in chemIMBA bioassay programs count median diameters, geometric standard deviations of particle size-distributions, and the total mass of each particle distribution needed to be determined.

The graphical aerosol spectra generated in the work done by Cheng and Jenkins were converted into tabular form. This tabular particle number concentration data was then input to MATLAB to acquire data-fits with a lognormal form. In order to generate lognormal distributions, rather than normal distributions, the base-ten logarithm of the particle diameters were taken and used as the horizontal data during the fitting process; the particle number concentrations were then plotted as a function of the log-base-ten of the particle diameter on the vertical axis. In MATLAB, each time dependent aerosol spectrum was then fit using single, or sums of, Gaussian functions with the following form:

$$Y = a * \exp(-\left(\frac{X-b}{c}\right)^2) \quad (6\text{-}1)$$

where X is the log-base-ten of the particle diameter, and Y is the number concentration of the particles of a given diameter. The coefficients a, b, and c are numerical values reported by MATLAB as a result of the fit. The resulting normal fits yielded the necessary lognormal particle distribution equations. The resultant MATLAB numerical output values of the fits for Blast B, Blast C, and Blast D can be viewed in Table 5, Table 6, and Table 7, respectively. Following the selection of each data-fit, the goodness of the fit was reported by MATLAB. The values of R-squared and root-mean-square-error associated with Blast B, Blast C, and Blast D, for each time-dependent size-distribution's fit, can be seen in Table 8, Table 9, and Table 10, respectively.

The MATLAB numerical values of outputs a, b, and c were then converted algebraically to obtain the needed Gaussian parameters, CMDs and geometric standard deviations of the particle distributions. The CMD of the lognormal distribution was derived from the MATLAB numerical output using the following form:

$$CMD = 10^b \quad (6\text{-}2)$$

The standard deviation of the lognormal distribution was derived from the MATLAB fit output using the following form:

$$\sigma_g = 10^{(\sqrt{(\frac{c^2}{2})})} \quad (6\text{-}3)$$

where σ_g is the geometric standard deviation. Values of CMD and σ_g for Blast B, Blast C, and Blast D, can be seen in Table 5, Table 6, and Table 7, respectively.

In order to integrate the particle spectra and, thus, determine the total mass of each distribution, the particle number concentrations generated by the fits had to be made functions of particle mass, rather than particle diameter.

The particle diameters were converted to particle masses assuming a density of one gram per cubic centimeter, and spherical shape:

$$m = \frac{4}{3} * \pi * \left(\frac{d}{2}\right)^3 * \rho \quad (6\text{-}4)$$

where m is the particle mass, d is the particle diameter, and ρ is the density. The equations of the number concentration fits were then made functions of mass using the following form

$$Y = a * \exp(-\left(\frac{log_{10}\left(2*\left(\frac{3*m}{4*\pi}\right)^{\frac{1}{3}}\right)-b}{c}\right)^2) \quad (6\text{-}5)$$

These functions of mass were then integrated numerically using the sum of two thousand five hundred and one trapezoid increments correlating to mass values associated with particle diameters ranging from zero nanometers to two thousand five hundred nanometers, in one nanometer increments. This broad range of data points was selected to safely include the entire spectrum of particle sizes contained in the aerosols. This function was integrated over the full range of particle masses in MATLAB using the trapezoidal function. The resulting integral is the total aerosol mass per volume of air for a given time interval for the given time-dependent, and bomb-dependent, size-distribution. These mass concentrations were then multiplied by the ICRP 66 reference inspiration rate for both light exercise (1.5 m^3/hr) and heavy exercise (3 m^3/hr); based on consideration of realistic exposure scenarios, light exercise was chosen to represent a laboratory worker, whereas heavy exercise inspiration was chosen to represent a soldier in the battlefield.[6] The resulting values are the total mass of particles inspired by a reference male, under both heavy and light exercise conditions, per unit time for each lognormal component of a given time-dependent, and blast-dependent, size-distribution. All size-distribution mass values for Blast B, Blast C, and Blast D can be seen in Table 11, Table 12, and Table 13, respectively.

In the application of these aerosol spectra, particle size-distributions used to represent a given period of exposure were often collected over smaller periods of time than they are being used to represent. This occurs, because of the limited temporal resolution of the applied aerosol size-distributions. For example, in the case of Blast B, the fit generated from particle number concentration data collected over a one minute interval from sixteen to seventeen minutes post-detonation was used to represent a seven minute exposure from eleven to eighteen minutes post-detonation.

Using the results of the spectral fits the size-distributions observed by Cheng & Jenkins were now able to be implemented as inputs in the chemIMBA software package.[19] In order to simulate realistic exposure scenarios, Dr. Charles M. Jenkins from the Air Force Research Laboratory (AFRL) was consulted regarding duration and conditions of potential human exposure to the aerosols.

B. Battle Field Exposure Scenarios

It was determined that a simulation of battlefield exposure should consist of a single extended period of exposure occurring immediately following a bomb's detonation. This extended period was selected to be one hour, based on consideration of aerosol spectral trends observed by Cheng and Jenkins in 2004; the vast majority of aerosols had completely settled, or had otherwise dissipated, within one hour post-detonation. Spectra simulated via the Cheng Jenkins data-fits were then selected to represent the particle distributions of aerosols present during all required post-detonation times of exposure.

The total mass of each spectral exposure was determined by calculating the product of the total mass of particles inspired by an ICRP reference male under heavy exercise conditions per unit time and the representative duration of exposure assigned to a given aerosol time-dependent size-distribution. In order to maximize the exposure-time accuracy of the inhalation simulation, once the total mass of a time-period's aerosol exposure was determined, each exposure was simulated in chemIMBA by delta function exposures at the midpoint of their representative time-

period. The choices of size-distribution's time-period representations for battlefield exposures for Blast B, Blast C, and Blast D can be viewed in Table 14, Table 15, and Table 16 respectively.

The battlefield scenarios for blast formulations B, C, and D were then simulated via chemIMBA. The mass of retention in several critical organs, and urinary excretion, for times ranging from a tenth of a day to ten thousand days post-detonation were predicted and exported in tabular form. These values were then normalized by the total mass of inhaled material in order to establish Intake Excretion Fractions (IEF) and Intake Retention Fractions (IRF). IRFs and IEFs for Blasts B, C, and D can be found in Table 17, Table 18, and Table 19, respectively. Graphical representation of the mass retention and excretion for Blasts, B, C, and D can be found in Figure 14, Figure 15, and Figure 16, respectively.

C. Laboratory Worker Exposure Scenarios

It was determined that a worker exposure in a bomb testing lab should consist of three separate aerosol exposures. The three exposure periods selected for worker exposure scenarios were determined based on the consultation of Dr. Charles M. Jenkins. The first of the three worker-exposure periods consists of a period starting five minutes after the explosive charge has been detonated. Workers are assumed to conduct their work in the blast chamber for a maximum duration of ten minutes; the first exposure simulation time-period is assumed to take place from five minutes post-detonation to fifteen minutes post-detonation. The workers then leave the chamber for a minimum of thirty minutes. After waiting thirty minutes, workers return to the blast chamber to clean the post detonation debris. This cleaning may last up to thirty minutes; the second exposure simulation period is assumed to take place from forty-five minutes post-detonation to seventy-five minutes post-detonation. After cleaning the chamber completely, the workers leave the chamber for approximately thirty minutes. After the thirty minute leave, the workers return for one and a half hours to setup the next blast. Based on trends of particle number concentration observed by Cheng and Jenkins, inhalation exposures during this third potential exposure period are assumed to be negligible. Spectra simulated via the aerosol size-distribution data-fits were then selected to represent the particle-distributions of aerosols present during all required post-detonation times of exposure.

The total mass of each aerosol exposure was determined by calculating the product of the total mass of particles inspired by an ICRP reference male under light exercise conditions per unit time and the representative duration of exposure assigned to a given aerosol time-dependent size-distribution. In order to maximize the exposure-time accuracy of the inhalation simulation, once the total mass of a time-period's exposure was determined, each exposure was simulated in chemIMBA by delta function exposures at the midpoint of their representative time-period. The choices of size-distribution's time-period representations for worker exposures for Blast B, Blast C, and Blast D can be viewed in Table 20, Table 21, and Table 22 respectively.

The worker scenarios for blast formulations B, C, and D were then simulated via chemIMBA. The mass of retention in several critical organs, and urinary excretion, for times ranging from a tenth of a day to ten thousand days post-detonation were predicted and exported in tabular form. These values were then normalized by the total mass of inhaled material in order to establish IEF and IRF. IRFs and IEFs for Blasts B, C, and D can be found in Tables 23, Table

24, and Table 25, respectively. Graphical representation of the mass retention and excretion for Blasts, B, C, and D can be found in Figure 17, Figure 18, and Figure 19, respectively.

D. Discussion of Exposure Scenario Simulations

As a result of the full simulation of inhalation exposures to both laboratory workers and soldiers in the battlefield it was found that the cumulative body burden of aluminum never exceeds values greater than a fifth of the total potentially up-taken particle mass. After further investigation regarding particle respiratory deposition, it was found that the average particle-sizes produced in the post-detonation munitions aerosols were extremely close to the minimum respiratory deposition sizes predicted by ICRP 66.[6] A graphical representation of this relationship is presented by Figure 20

Table 5. Data-fit parameters produced from Blast B size-distributions

t-PD[a] (min)	a	b	c	CMD (nm)	σ_g
1	2.72E+06	2.02E+00	1.16E-01	104.47	1.21
1	2.91E+06	2.12E+00	3.19E-01	130.32	1.68
1	2.28E+06	1.55E+00	2.56E-01	35.08	1.52
2	1.28E+06	2.05E+00	3.91E-01	112.46	1.89
6	9.38E+05	2.42E+00	1.54E-01	265.46	1.29
6	4.47E+05	2.18E+00	3.06E-01	150.66	1.65
17	1.09E+06	2.37E+00	2.97E-01	232.27	1.62
20	7.96E+05	2.38E+00	3.27E-01	238.23	1.70
41	1.80E+05	2.41E+00	2.27E-01	255.86	1.45
41	7.28E+04	1.97E+00	3.03E-01	92.47	1.64

[a] t-PD is the time post-detonation that the given size-distribution measurement was concluded. In situations where a size-distribution was represented by multiple lognormal components, each lognormal component's parameters are listed separately. All size-distributions for Blast B were measured over 1 minute intervals.

Table 6. Data-fit parameters produced from Blast C size-distributions

t-PD[a] (min)	a	b	c	CMD (nm)	σ_g
1	9.00E+06	1.62E+00	1.31E-01	41.40	1.24
1	4.05E+06	1.82E+00	2.57E-01	66.07	1.52
3	1.89E+06	2.11E+00	3.16E-01	130.02	1.67
3	7.11E+05	1.53E+00	8.33E-01	33.81	3.88
5	2.52E+06	2.19E+00	3.90E-01	153.11	1.89
9	2.19E+06	2.52E+00	1.88E-01	331.13	1.36
9	2.73E+06	2.22E+00	2.75E-01	165.58	1.56
20	1.60E+06	2.40E+00	3.99E-01	251.19	1.91
25	9.22E+05	2.43E+00	4.17E-01	266.69	1.97

[a] t-PD is the time post-detonation that the given size-distribution measurement was concluded. In situations where a size-distribution was represented by multiple lognormal components, each lognormal component's parameters are listed separately. All size-distributions for Blast C were measured over 1 minute intervals.

Table 7. Data-fit parameters produced from Blast D size-distributions

t-PD[a] (min)	a	b	c	CMD (nm)	σ_g
1.5	8.87E+06	1.61E+00	1.12E-01	40.93	1.20
1.5	3.60E+06	1.75E+00	1.93E-01	55.72	1.37
1.5	3.65E+05	1.80E+00	8.70E-02	62.95	1.15
3.0	4.60E+05	1.96E+00	1.95E-01	90.57	1.37
3.0	7.23E+05	1.64E+00	5.24E-01	43.25	2.35
10.5	9.07E+05	2.00E+00	2.96E-01	99.08	1.62
19.5	3.92E+05	2.07E+00	3.14E-01	117.22	1.67
30.0	1.28E+05	2.26E+00	1.51E-01	182.81	1.28
30.0	2.30E+05	2.02E+00	2.28E-01	104.71	1.45
40.5	2.55E+05	2.09E+00	3.11E-01	123.31	1.66

[a] t-PD is the time post-detonation that the given size-distribution measurement was concluded. In situations where a size-distribution was represented by multiple lognormal components, each lognormal component's parameters are listed separately. All size-distributions for Blast D were measured over 1.5 minute intervals.

Table 8. Goodness of fit for Blast B size-distributions

t -PD[a] (min)	R^2	RMSE (#/cm^3)
1	0.993	1.35E+05
2	0.989	4.68E+04
6	0.976	6.29E+04
17	0.935	8.57E+04
20	0.963	5.95E+04
41	0.962	1.33E+04

[a] t-PD is the time post-detonation that the given size-distribution measurement was concluded. All size-distributions for Blast B were measured over 1 minute intervals.

Table 9. Goodness of fit for Blast C size-distributions

t -PD[a] (min)	R^2	RMSE (#/cm^3)
1	0.984	4.80E+05
3	0.956	1.39E+05
5	0.950	1.94E+05
9	0.954	2.73E+05
20	0.985	7.22E+04
25	0.973	5.58E+04

[a] t-PD is the time post-detonation that the given size-distribution measurement was concluded. All size-distributions for Blast C were measured over 1 minute intervals.

Table 10. Goodness of fit for Blast D size-distributions

t -PD[a] (min)	R^2	RMSE (#/cm^3)
1.5	0.991	4.16E+05
3.0	0.977	6.14E+04
10.5	0.948	7.35E+04
19.5	0.980	1.74E+04
30.0	0.815	3.87E+04
40.5	0.901	2.90E+04

[a] t-PD is the time post-detonation that the given size-distribution measurement was concluded. All size-distributions for Blast D were measured over 1.5 minute intervals.

Table 11. Size-distribution masses and mass-inhalation rates for Blast B

t-PD[a]	Mass-concentration (g/cm^3)	Soldier mass-inhalation rate (mg/min)	Worker mass-inhalation rate (mg/min)
1	2.70E-09	1.35E-01	6.75E-02
1	4.42E-08	2.21E+00	1.10E+00
1	3.54E-10	1.77E-02	8.86E-03
2	2.81E-08	1.41E+00	7.03E-01
6	2.31E-08	1.15E+00	5.77E-01
6	9.18E-09	4.59E-01	2.29E-01
17	7.41E-08	3.70E+00	1.85E+00
20	8.07E-08	4.04E+00	2.02E+00
41	8.15E-09	4.08E-01	2.04E-01
41	3.33E-10	1.67E-02	8.33E-03

[a] t-PD is the time post-detonation that the given size-distribution measurement was concluded. In situations where a size-distribution was represented by multiple lognormal components, each lognormal component's parameters are listed separately. All size-distributions for Blast B were measured over 1 minute intervals.

Table 12. Size-distribution masses and mass-inhalation rates for Blast C

t-PD[a]	Mass-concentration (g/cm^3)	Soldier mass inhalation rate (mg/min)	Worker mass inhalation rate (mg/min)
1	6.61E-10	3.31E-02	1.65E-02
1	4.23E-09	2.12E-01	1.06E-01
3	2.76E-08	1.38E+00	6.89E-01
3	1.07E-07	5.36E+00	2.68E+00
5	1.38E-07	6.89E+00	3.45E+00
9	1.46E-07	7.30E+00	3.65E+00
9	5.37E-08	2.68E+00	1.34E+00
20	4.07E-07	2.03E+01	1.02E+01
25	3.32E-07	1.66E+01	8.30E+00

[a] t-PD is the time post-detonation that the given size-distribution measurement was concluded. In situations where a size-distribution was represented by multiple lognormal components, each lognormal component's parameters are listed separately. All size-distributions for Blast C were measured over 1 minute intervals.

Table 13. Size-distribution masses and mass-inhalation rates for Blast D

t-PD[a]	Mass-concentration (g/cm^3)	Soldier Mass Inhalation Rate (mg/min)	Worker Mass Inhalation Rate (mg/min)
1.5	5.05E-10	1.68E-02	8.42E-03
1.5	1.97E-09	6.56E-02	3.28E-02
3.0	5.56E-11	1.85E-03	9.26E-04
3.0	6.73E-10	2.24E-02	1.12E-02
3.0	5.10E-09	1.70E-01	8.50E-02
10.5	4.75E-09	1.58E-01	7.92E-02
19.5	4.11E-09	1.37E-01	6.85E-02
30.0	9.86E-10	3.29E-02	1.64E-02
30.0	7.16E-10	2.39E-02	1.19E-02
40.5	3.01E-09	1.00E-01	5.02E-02

[a] t-PD is the time post-detonation that the given size-distribution measurement was concluded. In situations where a size-distribution was represented by multiple lognormal components, each lognormal component's parameters are listed separately. All size-distributions for Blast D were measured over 1.5 minute intervals.

Table 14. Size-distribution representations for battlefield exposure to Blast B

Simulated period of exposure (minutes post-detonation)	Collection period of representative data (minutes post-detonation)	Representative duration of exposure to representative data-fit (minutes)	Time of representative delta-function exposure (minutes post-detonation)
0.0 to 1.5	0 to 1	1.5	0.75
1.5 to 3.5	1 t o2	2	2.25
3.5 to 11	5 to 6	7.5	7.75
11 to 18	16 to 17	7	14.5
18 to 30	19 to 20	12	24
30 to 60	40 to 41	26	45

Table 15. Size-distribution representations for battlefield exposure to Blast C

Simulated period of exposure (minutes post-detonation)	Collection period of representative data (minutes post-detonation)	Representative duration of exposure to representative data-fit (minutes)	Time of representative delta-function exposure (minutes post-detonation)
0 to 1.5	0 to 1	1.5	0.75
1.5 to 3.5	2 to 3	2	2.5
3.5 to 6.5	4 to 5	3	5
6.5 to 14	8 to 9	7.5	10.25
14 to 22	19 to 20	8	18
22 to 60	24 to 25	20	41

Table 16. Size-distribution representations for battlefield exposure to Blast D

Simulated period of exposure (minutes post-detonation)	Collection period of representative data (minutes post-detonation)	Representative duration of exposure to representative data-fit (minutes)	Time of representative delta-function exposure (minutes post-detonation)
0 to 1.5	0 to 1.5	1.5	0.75
1.5 to 6	1.5 to 3	4.5	3.75
6 to 14.25	9 to 10.5	8.25	10.125
14.25 to 24	18 to 19.5	9.75	19.125
24 to 34.5	28.5 to 30	10.5	29.25
34.5 to 60	39 to 40.5	15.5	47.25

Table 17. IRF and IEF values for battlefield exposures to Blast B

Time post exposure (days)	Blood IRF	Liver and Spleen IRF	Bone IRF	Kidney IRF	Urine IEF
1.00E-01	2.81E-02	3.30E-02	4.79E-03	7.38E-03	2.60E-03
2.00E-01	1.67E-02	3.78E-02	7.21E-03	1.10E-02	6.58E-03
3.00E-01	1.39E-02	3.74E-02	9.00E-03	1.37E-02	9.59E-03
4.00E-01	1.19E-02	3.59E-02	1.05E-02	1.59E-02	1.20E-02
5.00E-01	1.04E-02	3.40E-02	1.18E-02	1.78E-02	1.40E-02
6.00E-01	9.09E-03	3.22E-02	1.30E-02	1.93E-02	1.57E-02
7.00E-01	7.98E-03	3.04E-02	1.40E-02	2.07E-02	1.72E-02
8.00E-01	7.03E-03	2.88E-02	1.49E-02	2.19E-02	1.85E-02
9.00E-01	6.20E-03	2.73E-02	1.56E-02	2.29E-02	1.96E-02
1.00E+00	5.48E-03	2.60E-02	1.63E-02	2.37E-02	2.06E-02
2.00E+00	1.81E-03	1.88E-02	2.02E-02	2.71E-02	2.62E-02
3.00E+00	8.42E-04	1.62E-02	2.16E-02	2.67E-02	2.82E-02
4.00E+00	5.81E-04	1.50E-02	2.24E-02	2.54E-02	2.93E-02
5.00E+00	5.01E-04	1.42E-02	2.30E-02	2.40E-02	3.01E-02
6.00E+00	4.67E-04	1.35E-02	2.36E-02	2.26E-02	3.09E-02
7.00E+00	4.45E-04	1.30E-02	2.41E-02	2.13E-02	3.16E-02
8.00E+00	4.26E-04	1.25E-02	2.47E-02	2.01E-02	3.23E-02
9.00E+00	4.08E-04	1.20E-02	2.52E-02	1.90E-02	3.29E-02
1.00E+01	3.91E-04	1.16E-02	2.56E-02	1.80E-02	3.36E-02
2.00E+01	2.50E-04	8.23E-03	2.93E-02	1.07E-02	3.85E-02
3.00E+01	1.65E-04	5.81E-03	3.17E-02	6.90E-03	4.17E-02
4.00E+01	1.13E-04	4.07E-03	3.33E-02	4.77E-03	4.39E-02
5.00E+01	8.04E-05	2.86E-03	3.43E-02	3.53E-03	4.55E-02
6.00E+01	5.95E-05	2.03E-03	3.51E-02	2.77E-03	4.66E-02
7.00E+01	4.56E-05	1.46E-03	3.57E-02	2.29E-03	4.75E-02
8.00E+01	3.60E-05	1.08E-03	3.61E-02	1.96E-03	4.81E-02
9.00E+01	2.93E-05	8.10E-04	3.64E-02	1.73E-03	4.87E-02
1.00E+02	2.44E-05	6.27E-04	3.66E-02	1.56E-03	4.92E-02
2.00E+02	7.77E-06	1.42E-04	3.72E-02	8.18E-04	5.17E-02
3.00E+02	4.37E-06	7.37E-05	3.69E-02	5.07E-04	5.28E-02
4.00E+02	3.39E-06	5.49E-05	3.63E-02	3.35E-04	5.36E-02
5.00E+02	3.06E-06	4.87E-05	3.57E-02	2.33E-04	5.42E-02
6.00E+02	2.90E-06	4.59E-05	3.51E-02	1.71E-04	5.47E-02
7.00E+02	2.79E-06	4.42E-05	3.46E-02	1.33E-04	5.52E-02
8.00E+02	2.70E-06	4.27E-05	3.40E-02	1.10E-04	5.57E-02
9.00E+02	2.62E-06	4.14E-05	3.35E-02	9.42E-05	5.61E-02
1.00E+03	2.54E-06	4.01E-05	3.29E-02	8.41E-05	5.65E-02
2.00E+03	1.89E-06	2.99E-05	2.84E-02	5.36E-05	6.00E-02
3.00E+03	1.45E-06	2.28E-05	2.50E-02	4.08E-05	6.27E-02

Table 17. Continued

Time post exposure (days)	Blood IRF	Liver and Spleen IRF	Bone IRF	Kidney IRF	Urine IEF
4.00E+03	1.14E-06	1.80E-05	2.24E-02	3.20E-05	6.47E-02
5.00E+03	9.21E-07	1.45E-05	2.03E-02	2.59E-05	6.64E-02
6.00E+03	7.67E-07	1.21E-05	1.85E-02	2.15E-05	6.77E-02
7.00E+03	6.55E-07	1.03E-05	1.71E-02	1.83E-05	6.88E-02
8.00E+03	5.71E-07	9.01E-06	1.58E-02	1.60E-05	6.98E-02
9.00E+03	5.07E-07	8.00E-06	1.47E-02	1.41E-05	7.07E-02
1.00E+04	4.56E-07	7.20E-06	1.37E-02	1.27E-05	7.14E-02

Table 18. IRF and IEF values for battlefield exposures to Blast C

Time post exposure (days)	Blood IRF	Liver and Spleen IRF	Bone IRF	Kidney IRF	Urine IEF
1.00E-01	3.35E-02	3.60E-02	5.14E-03	7.92E-03	2.64E-03
2.00E-01	1.89E-02	4.24E-02	7.93E-03	1.21E-02	7.14E-03
3.00E-01	1.56E-02	4.21E-02	9.95E-03	1.51E-02	1.05E-02
4.00E-01	1.34E-02	4.05E-02	1.17E-02	1.76E-02	1.32E-02
5.00E-01	1.17E-02	3.84E-02	1.31E-02	1.97E-02	1.55E-02
6.00E-01	1.02E-02	3.63E-02	1.44E-02	2.15E-02	1.74E-02
7.00E-01	8.95E-03	3.44E-02	1.56E-02	2.30E-02	1.91E-02
8.00E-01	7.87E-03	3.26E-02	1.65E-02	2.43E-02	2.05E-02
9.00E-01	6.94E-03	3.09E-02	1.74E-02	2.54E-02	2.18E-02
1.00E+00	6.14E-03	2.95E-02	1.82E-02	2.64E-02	2.29E-02
2.00E+00	2.01E-03	2.14E-02	2.25E-02	3.02E-02	2.91E-02
3.00E+00	9.36E-04	1.85E-02	2.41E-02	2.97E-02	3.14E-02
4.00E+00	6.46E-04	1.71E-02	2.50E-02	2.83E-02	3.26E-02
5.00E+00	5.57E-04	1.62E-02	2.57E-02	2.67E-02	3.36E-02
6.00E+00	5.20E-04	1.55E-02	2.63E-02	2.52E-02	3.44E-02
7.00E+00	4.96E-04	1.48E-02	2.69E-02	2.37E-02	3.52E-02
8.00E+00	4.75E-04	1.42E-02	2.75E-02	2.24E-02	3.60E-02
9.00E+00	4.55E-04	1.37E-02	2.80E-02	2.12E-02	3.67E-02
1.00E+01	4.36E-04	1.32E-02	2.85E-02	2.00E-02	3.74E-02
2.00E+01	2.80E-04	9.41E-03	3.27E-02	1.20E-02	4.29E-02
3.00E+01	1.84E-04	6.65E-03	3.53E-02	7.70E-03	4.65E-02
4.00E+01	1.26E-04	4.67E-03	3.71E-02	5.33E-03	4.90E-02
5.00E+01	9.02E-05	3.28E-03	3.83E-02	3.95E-03	5.07E-02
6.00E+01	6.67E-05	2.33E-03	3.91E-02	3.10E-03	5.19E-02
7.00E+01	5.11E-05	1.68E-03	3.98E-02	2.56E-03	5.29E-02
8.00E+01	4.04E-05	1.24E-03	4.02E-02	2.19E-03	5.37E-02
9.00E+01	3.28E-05	9.32E-04	4.06E-02	1.93E-03	5.43E-02

Table 18. Continued

Time post exposure (days)	Blood IRF	Liver and Spleen IRF	Bone IRF	Kidney IRF	Urine IEF
1.00E+02	2.73E-05	7.21E-04	4.08E-02	1.74E-03	5.48E-02
2.00E+02	8.66E-06	1.62E-04	4.15E-02	9.12E-04	5.76E-02
3.00E+02	4.86E-06	8.39E-05	4.11E-02	5.66E-04	5.89E-02
4.00E+02	3.77E-06	6.24E-05	4.05E-02	3.73E-04	5.97E-02
5.00E+02	3.40E-06	5.54E-05	3.99E-02	2.59E-04	6.04E-02
6.00E+02	3.22E-06	5.23E-05	3.92E-02	1.91E-04	6.10E-02
7.00E+02	3.10E-06	5.03E-05	3.85E-02	1.48E-04	6.16E-02
8.00E+02	3.00E-06	4.86E-05	3.79E-02	1.22E-04	6.21E-02
9.00E+02	2.91E-06	4.71E-05	3.73E-02	1.05E-04	6.26E-02
1.00E+03	2.82E-06	4.56E-05	3.67E-02	9.35E-05	6.30E-02
2.00E+03	2.10E-06	3.40E-05	3.17E-02	5.95E-05	6.69E-02
3.00E+03	1.61E-06	2.60E-05	2.79E-02	4.53E-05	6.99E-02
4.00E+03	1.26E-06	2.04E-05	2.49E-02	3.56E-05	7.21E-02
5.00E+03	1.02E-06	1.65E-05	2.26E-02	2.88E-05	7.40E-02
6.00E+03	8.52E-07	1.37E-05	2.07E-02	2.39E-05	7.55E-02
7.00E+03	7.27E-07	1.17E-05	1.90E-02	2.03E-05	7.67E-02
8.00E+03	6.34E-07	1.02E-05	1.76E-02	1.77E-05	7.78E-02
9.00E+03	5.63E-07	9.07E-06	1.64E-02	1.57E-05	7.87E-02
1.00E+04	5.06E-07	8.17E-06	1.52E-02	1.41E-05	7.96E-02

Table 19. IRF and IEF values for battlefield exposures to Blast D

Time post exposure (days)	Blood IRF	Liver and Spleen IRF	Bone IRF	Kidney IRF	Urine IEF
1.00E-01	4.98E-02	5.77E-02	8.39E-03	1.29E-02	4.59E-03
2.00E-01	2.94E-02	6.64E-02	1.27E-02	1.94E-02	1.16E-02
3.00E-01	2.44E-02	6.57E-02	1.58E-02	2.40E-02	1.68E-02
4.00E-01	2.10E-02	6.30E-02	1.85E-02	2.79E-02	2.10E-02
5.00E-01	1.82E-02	5.98E-02	2.08E-02	3.12E-02	2.45E-02
6.00E-01	1.59E-02	5.65E-02	2.28E-02	3.40E-02	2.75E-02
7.00E-01	1.40E-02	5.34E-02	2.45E-02	3.63E-02	3.01E-02
8.00E-01	1.23E-02	5.06E-02	2.61E-02	3.84E-02	3.24E-02
9.00E-01	1.09E-02	4.80E-02	2.75E-02	4.01E-02	3.44E-02
1.00E+00	9.62E-03	4.57E-02	2.87E-02	4.16E-02	3.62E-02
2.00E+00	3.17E-03	3.30E-02	3.54E-02	4.75E-02	4.59E-02
3.00E+00	1.48E-03	2.86E-02	3.79E-02	4.68E-02	4.95E-02
4.00E+00	1.02E-03	2.64E-02	3.93E-02	4.45E-02	5.14E-02
5.00E+00	8.79E-04	2.49E-02	4.04E-02	4.21E-02	5.29E-02
6.00E+00	8.20E-04	2.38E-02	4.14E-02	3.97E-02	5.42E-02
7.00E+00	7.82E-04	2.28E-02	4.24E-02	3.74E-02	5.55E-02

Table 19. Continued

Time post exposure (days)	Blood IRF	Liver and Spleen IRF	Bone IRF	Kidney IRF	Urine IEF
8.00E+00	7.48E-04	2.19E-02	4.33E-02	3.53E-02	5.67E-02
9.00E+00	7.17E-04	2.11E-02	4.41E-02	3.34E-02	5.78E-02
1.00E+01	6.86E-04	2.04E-02	4.50E-02	3.16E-02	5.89E-02
2.00E+01	4.39E-04	1.45E-02	5.15E-02	1.89E-02	6.76E-02
3.00E+01	2.89E-04	1.02E-02	5.56E-02	1.21E-02	7.32E-02
4.00E+01	1.98E-04	7.16E-03	5.84E-02	8.37E-03	7.71E-02
5.00E+01	1.41E-04	5.03E-03	6.03E-02	6.20E-03	7.98E-02
6.00E+01	1.04E-04	3.57E-03	6.16E-02	4.87E-03	8.18E-02
7.00E+01	8.00E-05	2.57E-03	6.26E-02	4.02E-03	8.33E-02
8.00E+01	6.32E-05	1.89E-03	6.33E-02	3.44E-03	8.45E-02
9.00E+01	5.14E-05	1.43E-03	6.38E-02	3.04E-03	8.55E-02
1.00E+02	4.27E-05	1.10E-03	6.42E-02	2.74E-03	8.63E-02
2.00E+02	1.36E-05	2.49E-04	6.53E-02	1.43E-03	9.07E-02
3.00E+02	7.67E-06	1.30E-04	6.47E-02	8.91E-04	9.27E-02
4.00E+02	5.95E-06	9.64E-05	6.38E-02	5.87E-04	9.40E-02
5.00E+02	5.36E-06	8.56E-05	6.27E-02	4.09E-04	9.51E-02
6.00E+02	5.08E-06	8.08E-05	6.17E-02	3.01E-04	9.60E-02
7.00E+02	4.90E-06	7.77E-05	6.07E-02	2.34E-04	9.69E-02
8.00E+02	4.74E-06	7.51E-05	5.97E-02	1.92E-04	9.77E-02
9.00E+02	4.59E-06	7.28E-05	5.87E-02	1.65E-04	9.85E-02
1.00E+03	4.45E-06	7.06E-05	5.78E-02	1.48E-04	9.92E-02
2.00E+03	3.31E-06	5.25E-05	4.99E-02	9.40E-05	1.05E-01
3.00E+03	2.54E-06	4.01E-05	4.39E-02	7.16E-05	1.10E-01
4.00E+03	2.00E-06	3.16E-05	3.93E-02	5.62E-05	1.14E-01

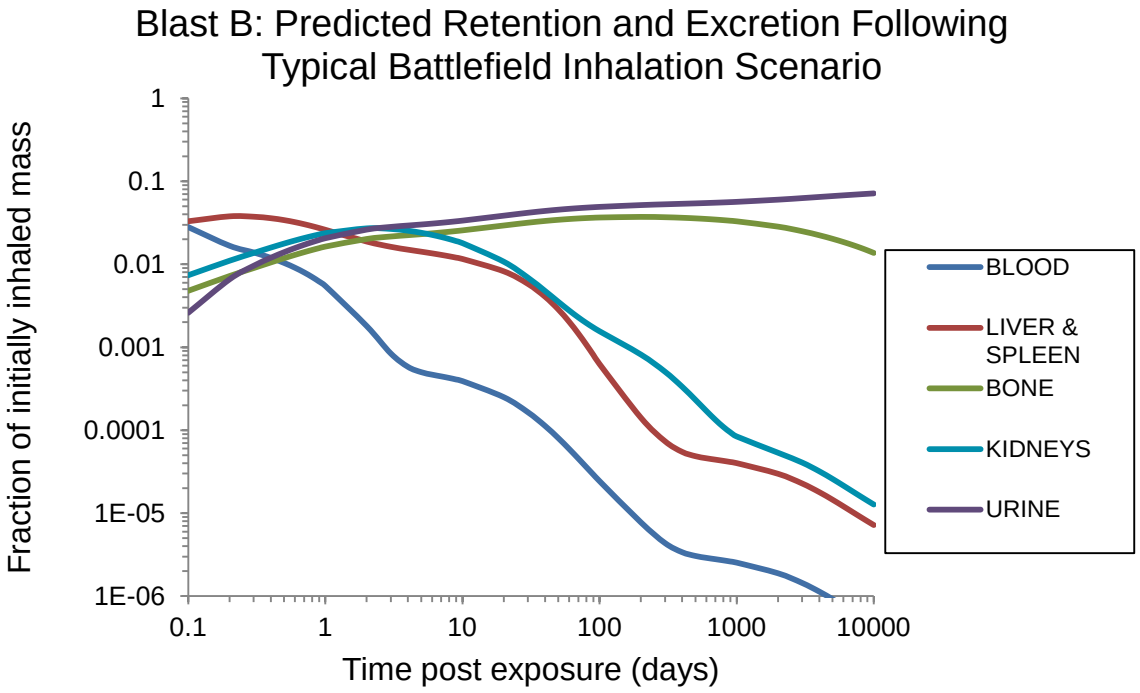

Figure 14. Biokinetic trends predicted by chemIMBA for a typical battlefield inhalation scenario following a detonation of an explosive containing Blast B formulation

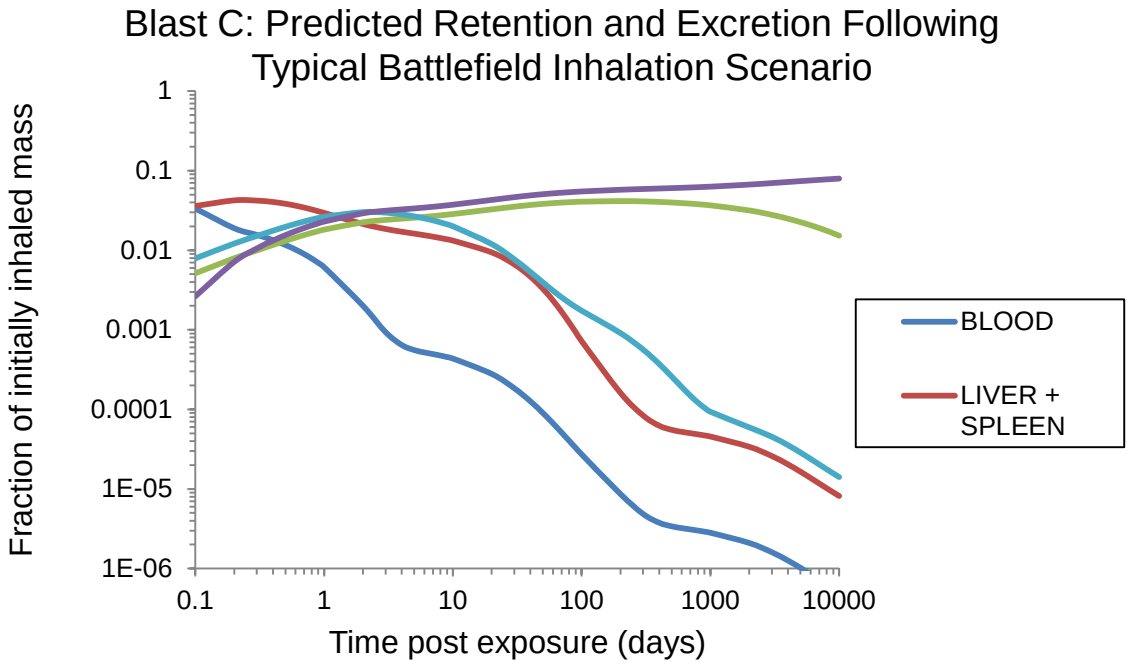

Figure 15. Biokinetic trends predicted by chemIMBA for a typical battlefield inhalation scenario following a detonation of an explosive containing Blast C formulation

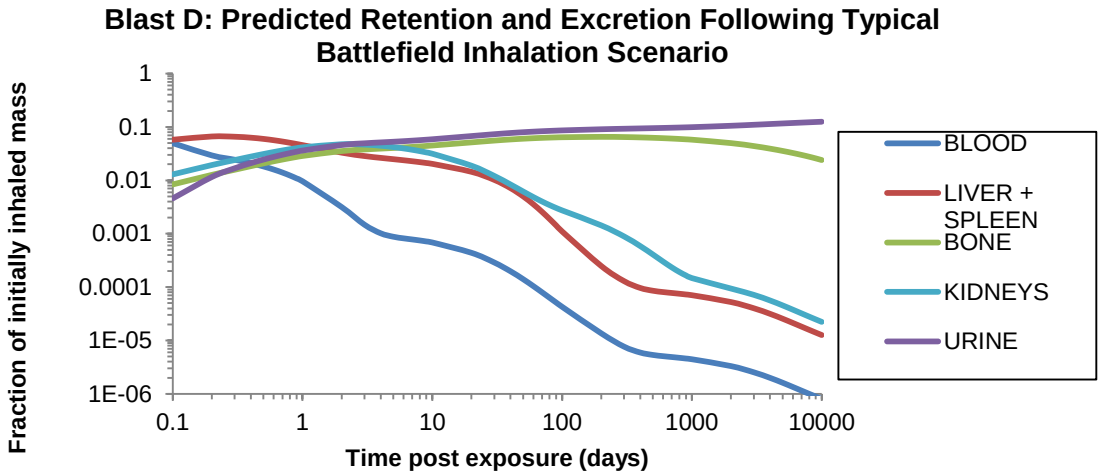

Figure 16. Biokinetic trends predicted by chemIMBA for a typical battlefield inhalation scenario following a detonation of an explosive containing Blast D formulation

Table 20. Size-distribution representations for worker exposure to Blast B

Simulated period of exposure (minutes post-detonation)	Collection period of representative data (minutes post-detonation)	Representative duration of exposure to representative data-fit (minutes)	Time of representative delta-function exposure (minutes post-detonation)
5 to 10.5	5 to 6	5.5	7.75
10.5 to 15	16 to 17	4.5	12.75
45 to 75	40 to 41	15	60

Table 21. Size-distribution representations for worker exposure to Blast C

Simulated period of exposure (minutes post-detonation)	Collection period of representative data (minutes post-detonation)	Representative duration of exposure to representative data-fit (minutes)	Time of representative delta-function exposure (minutes post-detonation)
5 to 7	4 to 5	2	6
7 to 12	8 to 9	5	9.5
12 to 15	19 to 20	3	13.5
45 to 75	24 to 25	8	60

Table 22. Size-distribution representations for worker exposure to Blast D

Simulated period of exposure (minutes post-detonation)	Collection period of representative data (minutes post-detonation)	Representative duration of exposure to representative data-fit (minutes)	Time of representative delta-function exposure (minutes post-detonation)
5 to 6	1.5 to 3.0	1	5.5
6 to 14	9.0 to 10.5	8	10
14 to 15	18.0 to 19.5	1	14.5
45 to 75	39 to 40.5	14	60

Table 23. IRF and IEF values for worker exposures to Blast B

Time post exposure [days]	Blood IRF	Liver and Spleen IRF	Bone IRF	Kidney IRF	Urine IEF
1.00E-01	2.79E-02	3.41E-02	4.67E-03	7.20E-03	2.55E-03
2.00E-01	1.60E-02	3.97E-02	7.03E-03	1.07E-02	6.43E-03
3.00E-01	1.31E-02	3.97E-02	8.73E-03	1.33E-02	9.32E-03
4.00E-01	1.12E-02	3.86E-02	1.02E-02	1.53E-02	1.16E-02
5.00E-01	9.64E-03	3.71E-02	1.14E-02	1.71E-02	1.35E-02
6.00E-01	8.36E-03	3.55E-02	1.24E-02	1.85E-02	1.51E-02
7.00E-01	7.28E-03	3.40E-02	1.34E-02	1.98E-02	1.64E-02
8.00E-01	6.35E-03	3.26E-02	1.42E-02	2.08E-02	1.76E-02
9.00E-01	5.56E-03	3.14E-02	1.49E-02	2.17E-02	1.87E-02
1.00E+00	4.88E-03	3.02E-02	1.55E-02	2.24E-02	1.96E-02
2.00E+00	1.51E-03	2.39E-02	1.88E-02	2.52E-02	2.44E-02
3.00E+00	7.01E-04	2.15E-02	2.00E-02	2.46E-02	2.61E-02
4.00E+00	5.02E-04	2.01E-02	2.07E-02	2.33E-02	2.70E-02
5.00E+00	4.47E-04	1.90E-02	2.12E-02	2.20E-02	2.78E-02
6.00E+00	4.24E-04	1.82E-02	2.17E-02	2.07E-02	2.84E-02
7.00E+00	4.08E-04	1.75E-02	2.22E-02	1.95E-02	2.91E-02
8.00E+00	3.94E-04	1.68E-02	2.27E-02	1.84E-02	2.97E-02
9.00E+00	3.79E-04	1.62E-02	2.31E-02	1.74E-02	3.03E-02
1.00E+01	3.65E-04	1.56E-02	2.36E-02	1.65E-02	3.09E-02
2.00E+01	2.42E-04	1.12E-02	2.71E-02	9.98E-03	3.56E-02
3.00E+01	1.64E-04	8.05E-03	2.94E-02	6.53E-03	3.87E-02
4.00E+01	1.14E-04	5.73E-03	3.10E-02	4.59E-03	4.09E-02
5.00E+01	8.26E-05	4.08E-03	3.21E-02	3.44E-03	4.25E-02
6.00E+01	6.14E-05	2.93E-03	3.29E-02	2.72E-03	4.37E-02
7.00E+01	4.70E-05	2.14E-03	3.35E-02	2.25E-03	4.45E-02
8.00E+01	3.69E-05	1.58E-03	3.39E-02	1.92E-03	4.52E-02
9.00E+01	2.97E-05	1.19E-03	3.42E-02	1.69E-03	4.58E-02

Table 23. Continued

Time post exposure [days]	Blood IRF	Liver and Spleen IRF	Bone IRF	Kidney IRF	Urine IEF
1.00E+02	2.44E-05	9.22E-04	3.45E-02	1.51E-03	4.63E-02
2.00E+02	7.17E-06	1.91E-04	3.51E-02	7.70E-04	4.87E-02
3.00E+02	3.94E-06	9.63E-05	3.47E-02	4.76E-04	4.97E-02
4.00E+02	3.03E-06	7.08E-05	3.42E-02	3.12E-04	5.04E-02
5.00E+02	2.72E-06	6.25E-05	3.36E-02	2.16E-04	5.10E-02
6.00E+02	2.58E-06	5.89E-05	3.30E-02	1.58E-04	5.14E-02
7.00E+02	2.48E-06	5.66E-05	3.25E-02	1.22E-04	5.19E-02
8.00E+02	2.40E-06	5.47E-05	3.19E-02	9.93E-05	5.23E-02
9.00E+02	2.32E-06	5.30E-05	3.14E-02	8.48E-05	5.27E-02
1.00E+03	2.25E-06	5.13E-05	3.09E-02	7.53E-05	5.31E-02
2.00E+03	1.67E-06	3.80E-05	2.65E-02	4.73E-05	5.62E-02
3.00E+03	1.27E-06	2.89E-05	2.33E-02	3.58E-05	5.85E-02
4.00E+03	9.92E-07	2.26E-05	2.08E-02	2.80E-05	6.03E-02
5.00E+03	8.00E-07	1.82E-05	1.88E-02	2.25E-05	6.17E-02
6.00E+03	6.64E-07	1.51E-05	1.71E-02	1.86E-05	6.29E-02
7.00E+03	5.65E-07	1.29E-05	1.57E-02	1.58E-05	6.38E-02
8.00E+03	4.91E-07	1.12E-05	1.45E-02	1.37E-05	6.47E-02
9.00E+03	4.35E-07	9.90E-06	1.35E-02	1.22E-05	6.54E-02
1.00E+04	3.91E-07	8.89E-06	1.26E-02	1.09E-05	6.61E-02

Table 24. IRF and IEF values for worker exposures to Blast C

Time post exposure [days]	Blood IRF	Liver and Spleen IRF	Bone IRF	Kidney IRF	Urine IEF
1.00E-01	3.60E-02	3.55E-02	4.74E-03	7.30E-03	2.30E-03
2.00E-01	1.84E-02	4.39E-02	7.57E-03	1.16E-02	6.71E-03
3.00E-01	1.49E-02	4.43E-02	9.51E-03	1.45E-02	1.00E-02
4.00E-01	1.27E-02	4.31E-02	1.11E-02	1.68E-02	1.26E-02
5.00E-01	1.09E-02	4.14E-02	1.25E-02	1.88E-02	1.48E-02
6.00E-01	9.44E-03	3.97E-02	1.37E-02	2.04E-02	1.66E-02
7.00E-01	8.22E-03	3.80E-02	1.47E-02	2.18E-02	1.81E-02
8.00E-01	7.17E-03	3.64E-02	1.57E-02	2.30E-02	1.95E-02
9.00E-01	6.27E-03	3.50E-02	1.64E-02	2.40E-02	2.06E-02
1.00E+00	5.50E-03	3.38E-02	1.71E-02	2.49E-02	2.17E-02
2.00E+00	1.69E-03	2.67E-02	2.09E-02	2.80E-02	2.71E-02
3.00E+00	7.84E-04	2.39E-02	2.22E-02	2.73E-02	2.90E-02
4.00E+00	5.60E-04	2.23E-02	2.30E-02	2.59E-02	3.00E-02
5.00E+00	4.97E-04	2.12E-02	2.36E-02	2.44E-02	3.09E-02
6.00E+00	4.72E-04	2.02E-02	2.42E-02	2.30E-02	3.16E-02

Table 24. Continued

Time post exposure [days]	Blood IRF	Liver and Spleen IRF	Bone IRF	Kidney IRF	Urine IEF
7.00E+00	4.54E-04	1.94E-02	2.47E-02	2.17E-02	3.23E-02
8.00E+00	4.38E-04	1.87E-02	2.52E-02	2.05E-02	3.30E-02
9.00E+00	4.22E-04	1.80E-02	2.57E-02	1.94E-02	3.37E-02
1.00E+01	4.06E-04	1.74E-02	2.62E-02	1.84E-02	3.43E-02
2.00E+01	2.69E-04	1.25E-02	3.01E-02	1.11E-02	3.96E-02
3.00E+01	1.82E-04	8.95E-03	3.27E-02	7.26E-03	4.31E-02
4.00E+01	1.27E-04	6.37E-03	3.45E-02	5.11E-03	4.55E-02
5.00E+01	9.18E-05	4.54E-03	3.57E-02	3.83E-03	4.72E-02
6.00E+01	6.83E-05	3.26E-03	3.66E-02	3.03E-03	4.85E-02
7.00E+01	5.22E-05	2.38E-03	3.72E-02	2.50E-03	4.95E-02
8.00E+01	4.10E-05	1.76E-03	3.77E-02	2.14E-03	5.03E-02
9.00E+01	3.30E-05	1.33E-03	3.80E-02	1.87E-03	5.09E-02
1.00E+02	2.71E-05	1.03E-03	3.83E-02	1.68E-03	5.14E-02
2.00E+02	7.97E-06	2.13E-04	3.90E-02	8.56E-04	5.41E-02
3.00E+02	4.38E-06	1.07E-04	3.86E-02	5.29E-04	5.53E-02
4.00E+02	3.37E-06	7.87E-05	3.80E-02	3.47E-04	5.61E-02
5.00E+02	3.02E-06	6.95E-05	3.74E-02	2.40E-04	5.67E-02
6.00E+02	2.86E-06	6.55E-05	3.67E-02	1.75E-04	5.72E-02
7.00E+02	2.76E-06	6.29E-05	3.61E-02	1.35E-04	5.77E-02
8.00E+02	2.67E-06	6.08E-05	3.55E-02	1.10E-04	5.81E-02
9.00E+02	2.58E-06	5.89E-05	3.49E-02	9.43E-05	5.86E-02
1.00E+03	2.50E-06	5.70E-05	3.43E-02	8.38E-05	5.90E-02
2.00E+03	1.85E-06	4.22E-05	2.95E-02	5.25E-05	6.24E-02
3.00E+03	1.41E-06	3.21E-05	2.59E-02	3.98E-05	6.50E-02
4.00E+03	1.10E-06	2.51E-05	2.31E-02	3.11E-05	6.70E-02
5.00E+03	8.90E-07	2.03E-05	2.08E-02	2.50E-05	6.86E-02
6.00E+03	7.38E-07	1.68E-05	1.90E-02	2.07E-05	6.99E-02
7.00E+03	6.28E-07	1.43E-05	1.75E-02	1.76E-05	7.10E-02
8.00E+03	5.46E-07	1.24E-05	1.62E-02	1.53E-05	7.19E-02
9.00E+03	4.84E-07	1.10E-05	1.50E-02	1.35E-05	7.27E-02
1.00E+04	4.35E-07	9.89E-06	1.40E-02	1.21E-05	7.35E-02

Table 25. IRF and IEF values for worker exposures to Blast D

Time post exposure [days]	Blood IRF	Liver and Spleen IRF	Bone IRF	Kidney IRF	Urine IEF
1.00E-01	5.30E-02	5.63E-02	7.60E-03	1.17E-02	3.89E-03
2.00E-01	2.81E-02	6.81E-02	1.19E-02	1.82E-02	1.07E-02
3.00E-01	2.29E-02	6.85E-02	1.48E-02	2.26E-02	1.57E-02
4.00E-01	1.95E-02	6.66E-02	1.73E-02	2.62E-02	1.97E-02
5.00E-01	1.68E-02	6.40E-02	1.95E-02	2.92E-02	2.30E-02
6.00E-01	1.45E-02	6.13E-02	2.13E-02	3.17E-02	2.58E-02
7.00E-01	1.26E-02	5.87E-02	2.29E-02	3.39E-02	2.81E-02
8.00E-01	1.10E-02	5.63E-02	2.43E-02	3.57E-02	3.02E-02
9.00E-01	9.66E-03	5.41E-02	2.55E-02	3.72E-02	3.20E-02
1.00E+00	8.47E-03	5.22E-02	2.66E-02	3.85E-02	3.36E-02
2.00E+00	2.61E-03	4.12E-02	3.23E-02	4.33E-02	4.20E-02
3.00E+00	1.21E-03	3.70E-02	3.44E-02	4.23E-02	4.49E-02
4.00E+00	8.66E-04	3.45E-02	3.56E-02	4.01E-02	4.65E-02
5.00E+00	7.69E-04	3.28E-02	3.65E-02	3.78E-02	4.78E-02
6.00E+00	7.30E-04	3.13E-02	3.74E-02	3.56E-02	4.89E-02
7.00E+00	7.03E-04	3.00E-02	3.82E-02	3.36E-02	5.01E-02
8.00E+00	6.78E-04	2.89E-02	3.90E-02	3.17E-02	5.11E-02
9.00E+00	6.53E-04	2.79E-02	3.98E-02	3.00E-02	5.22E-02
1.00E+01	6.28E-04	2.69E-02	4.06E-02	2.84E-02	5.32E-02
2.00E+01	4.16E-04	1.93E-02	4.66E-02	1.72E-02	6.12E-02
3.00E+01	2.82E-04	1.38E-02	5.06E-02	1.12E-02	6.67E-02
4.00E+01	1.97E-04	9.86E-03	5.34E-02	7.90E-03	7.04E-02
5.00E+01	1.42E-04	7.03E-03	5.53E-02	5.92E-03	7.31E-02
6.00E+01	1.06E-04	5.05E-03	5.66E-02	4.68E-03	7.51E-02
7.00E+01	8.08E-05	3.68E-03	5.76E-02	3.87E-03	7.66E-02
8.00E+01	6.35E-05	2.72E-03	5.83E-02	3.31E-03	7.78E-02
9.00E+01	5.11E-05	2.06E-03	5.89E-02	2.90E-03	7.88E-02
1.00E+02	4.20E-05	1.59E-03	5.93E-02	2.60E-03	7.96E-02
2.00E+02	1.23E-05	3.29E-04	6.04E-02	1.33E-03	8.37E-02
3.00E+02	6.78E-06	1.66E-04	5.98E-02	8.19E-04	8.56E-02
4.00E+02	5.21E-06	1.22E-04	5.89E-02	5.37E-04	8.68E-02
5.00E+02	4.68E-06	1.08E-04	5.79E-02	3.71E-04	8.77E-02
6.00E+02	4.43E-06	1.01E-04	5.69E-02	2.71E-04	8.85E-02
7.00E+02	4.27E-06	9.74E-05	5.59E-02	2.10E-04	8.93E-02
8.00E+02	4.13E-06	9.41E-05	5.50E-02	1.71E-04	9.00E-02
9.00E+02	4.00E-06	9.11E-05	5.40E-02	1.46E-04	9.06E-02
1.00E+03	3.87E-06	8.83E-05	5.32E-02	1.30E-04	9.13E-02
2.00E+03	2.87E-06	6.53E-05	4.57E-02	8.13E-05	9.66E-02

Table 25. Continued

Time post exposure [days]	Blood IRF	Liver and Spleen IRF	Bone IRF	Kidney IRF	Urine IEF
3.00E+03	2.18E-06	4.97E-05	4.01E-02	6.16E-05	1.01E-01
4.00E+03	1.71E-06	3.89E-05	3.57E-02	4.81E-05	1.04E-01
5.00E+03	1.38E-06	3.13E-05	3.23E-02	3.87E-05	1.06E-01
6.00E+03	1.14E-06	2.60E-05	2.94E-02	3.20E-05	1.08E-01
7.00E+03	9.72E-07	2.21E-05	2.71E-02	2.72E-05	1.10E-01
8.00E+03	8.46E-07	1.92E-05	2.50E-02	2.36E-05	1.11E-01
9.00E+03	7.49E-07	1.70E-05	2.32E-02	2.09E-05	1.13E-01
1.00E+04	6.73E-07	1.53E-05	2.16E-02	1.88E-05	1.14E-01

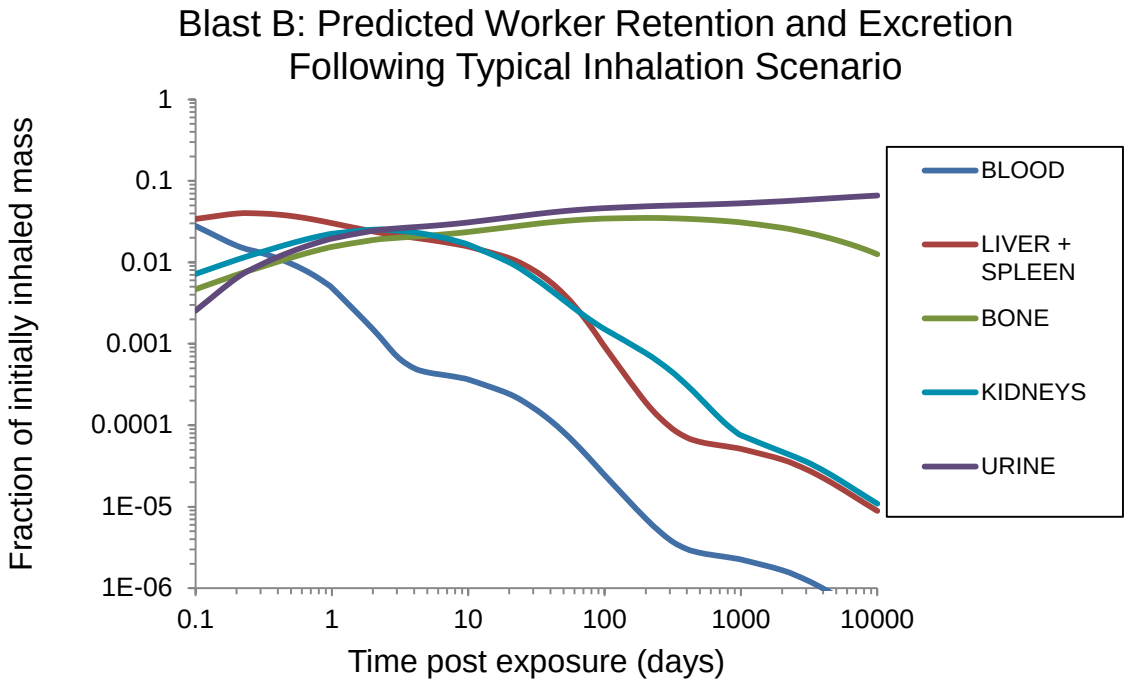

Figure 17. Biokinetic trends predicted by chemIMBA for a typical laboratory inhalation scenario following a detonation of an explosive containing Blast B formulation

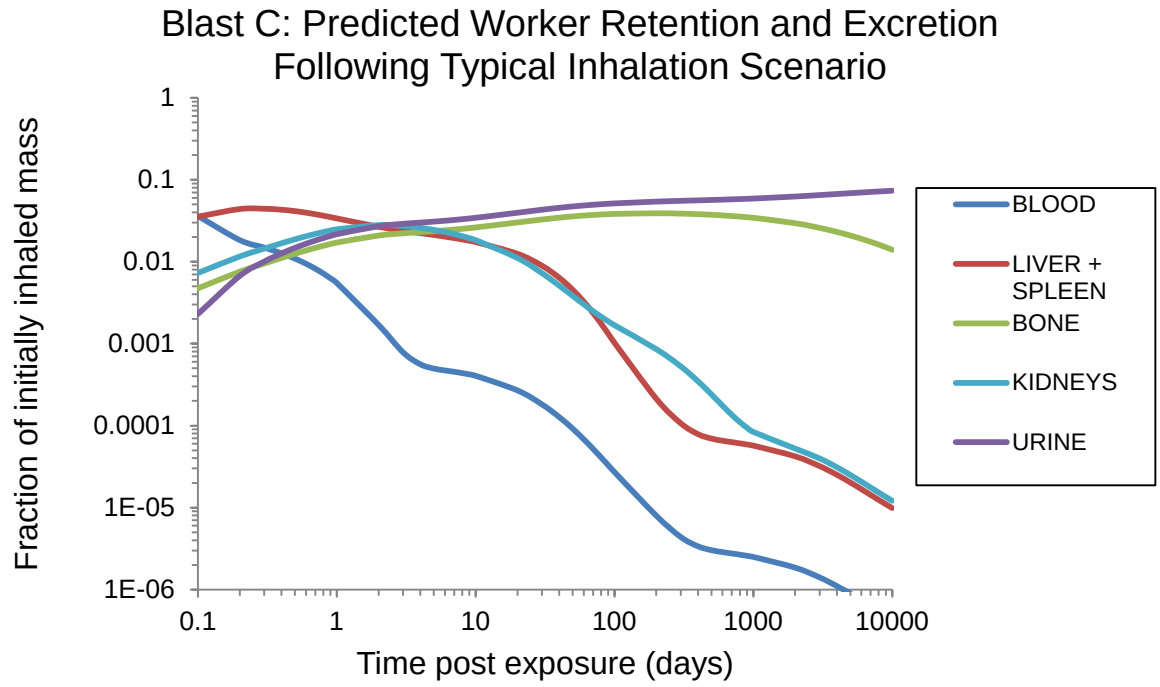

Figure 18. Biokinetic trends predicted by chemIMBA for a typical laboratory inhalation scenario following a detonation of an explosive containing Blast C formulation

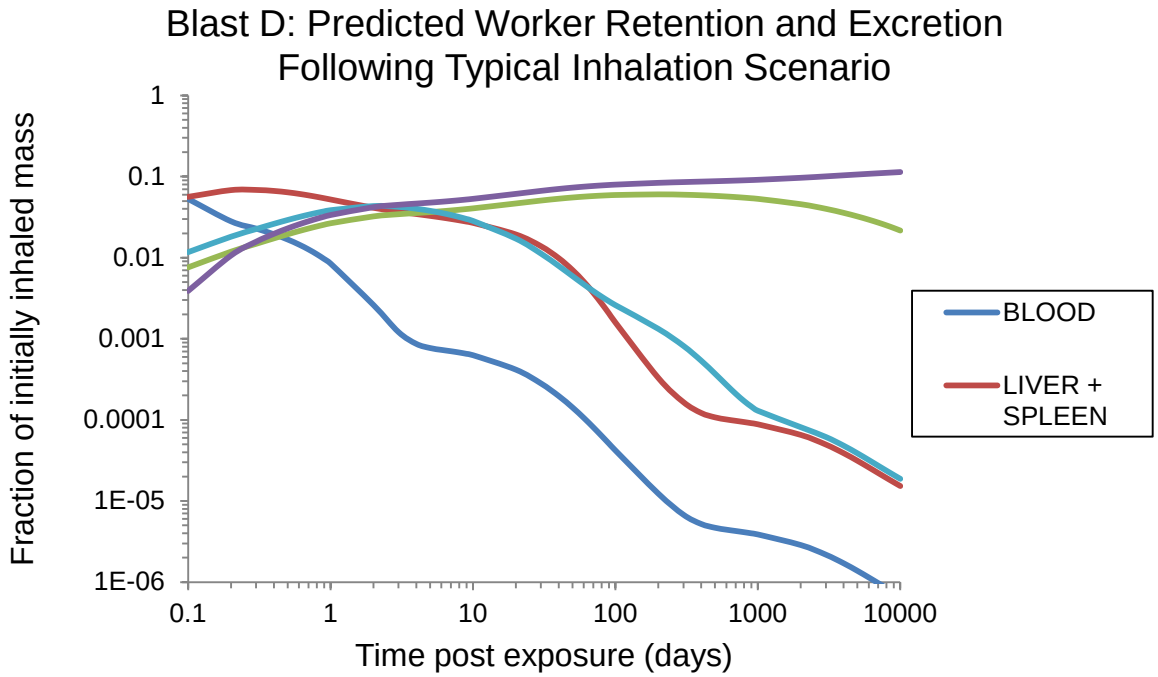

Figure 19. Biokinetic trends predicted by chemIMBA for a typical laboratory inhalation scenario following a detonation of an explosive containing Blast D formulation

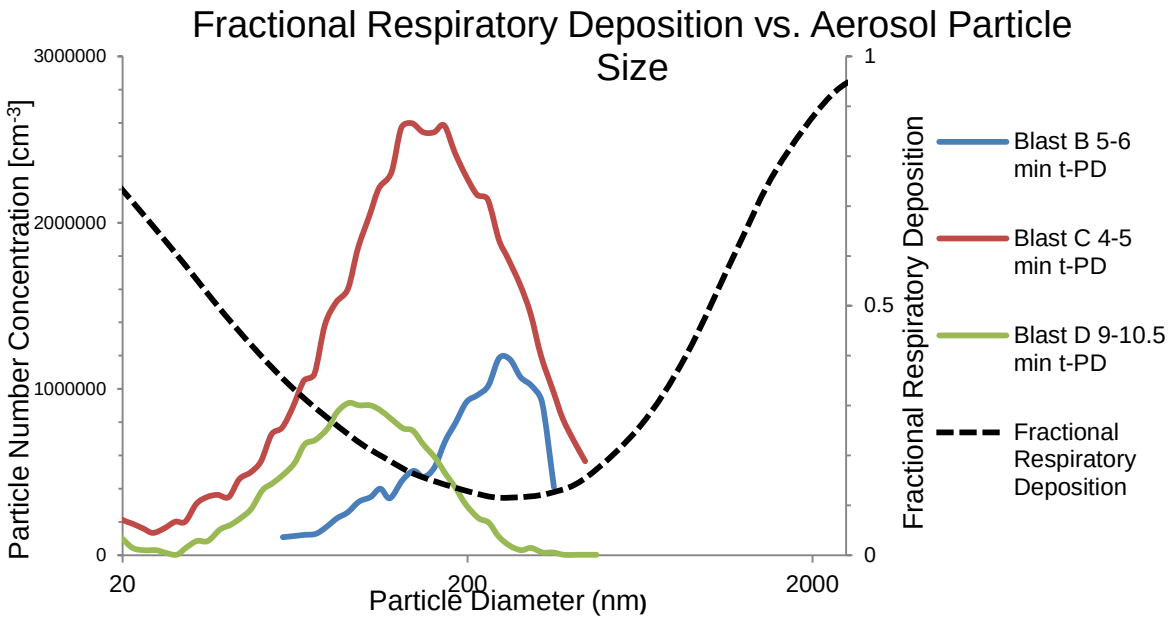

Figure 20. ICRP 66 fractional respiratory deposition particle size-dependence compared with representative blast size-distributions

7. CONCLUSIONS AND FUTURE WORK

A. Potential Improvements to Fundamentals of chemIMBA Software Package

The chemIMBA software does a vast amount to accurately predict the retention, and excretion of materials in the human body. However, when simulating the human alimentary tract, there is potential room for improvement. ChemIMBA makes use of the alimentary tract model developed in ICRP publication 30.[7] This model has since been improved with the creation of the ICRP 100 Human Alimentary Tract Model.[17] The new model's improvements include more explicit retention in the walls of the tract, and higher anatomical resolution. Furthermore, the model now incorporates the age, sex, and material-dependence of transfer rates. Implementation of this alimentary tract model would further improve the prediction accuracy of the chemIMBA software package, and bring it up to speed with state-of-the-art inhalation and ingestion prediction capabilities.

With the understanding that airborne particulate deposition is strongly dependent on the size of the particles being deposited, it can be seen that improvements in the accuracy of the size-distributions will lead to better bioassay estimates. Improving chemIMBA's provides a capability to accurately simulate the exposure-time of a given size-distribution would improve the accuracy of exposure bioassay predictions. In order to allow for more accurate simulation of the aerosol spectral time-dependence, chemIMBA needs to allow for a higher number of spectra inputs per exposure simulation.

The current edition of the software package is limited to a maximum of ten individual lognormal particle size-distributions as inputs to represent an entire exposure scenario. In many cases, a single time-dependent spectrum requires multiple lognormal components to be reasonably approximated. Furthermore, potential future exposure scenarios, and current exposures of workers, may consist of multiple separate isolated exposures separated by a variable length of time with no exposure to the aerosol of concern. The combination of these issues creates a situation where the time-dependent size-distributions of blast aerosols must be summed over large time periods of exposure and simulated as delta-function exposures for chemIMBA implementation. This leads to a reduction in the accuracy of the time of exposure to the individual time-dependent size-distributions of the aerosol. In short-term exposure monitoring this could impact the exposure results significantly. Further work analyzing the effects of the issue of this loss of exposure time-accuracy in bioassay predictions, and work to increase the number of potential chemIMBA spectra inputs, would help improve the bioassay capabilities of this program.

B. Acquire Element Specific Aerosol Size Distribution Data

The particle distribution data used to represent the exposures of both workers in laboratory environments, and soldiers in the battlefield, could use refining in several areas. Within the nanophase aluminum blast scenarios, the aerosol spectra generated after detonation of a test-charge potentially contain several pure elemental components, metal alloys, and even particles generated by the material in the area surrounding the explosive itself. If chemical analysis of the particles are provided insight as to which components of the particle distribution are composed of the element of interest versus the many other constituent particulate

components generated in the post-detonation aerosol could be determined. If chemical analysis were performed on these aerosols while maintaining knowledge on the size-distribution of the specific element's aerosol, it would greatly enhance the accuracy of the future aerosol exposure predictions.

Preliminary simulations of aluminum exposures were successfully simulated using post-detonation aerosol data studied by Cheng and Jenkins, but, in order to fully simulate all potential human exposures, aerosol size-distribution information needs to be gathered regarding the remaining four elements of interest. Work done to present any insight on the particle spectra produced by charges that contain formulations of these elements would aide greatly in comprehensively predicting any effects of human exposures in Air Force munitions development.

C. Refine Biokinetic Models of Elements of Interest

All elements considered for potential use in munitions development by The United States Air Force have limited biokinetic data available. The biokinetic models currently applied in the exposure bioassay monitoring procedures outlined in this paper are preliminary. The models being used have varying levels of reliability based on the amount of previous work done studying the biokinetics of these elements.

In the cases of boron, tantalum, and titanium extremely limited biokinetic data is available. Animal biokinetic studies and in-depth analysis of the viability of physiological, and chemical, analogues would be the most available avenue for model improvement. Aluminum biokinetics are fairly well developed; aluminum biokinetic data is at an intermediate point of prediction capabilities. Limited human data exists, but has led to validation of urinary excretion and blood uptake trends simulated by current systemic biokinetic models. However, retention of systemic aluminum could have much improved anatomical resolution granted the continuation of human studies. Specifically the kidney retention in healthy test subjects could be of great use in further model refinement.

Tungsten's current model structures, and transfer rates, have been well established on the basis of physiological considerations of animal studies and biological analogues, but the need for increased human validation does exist. The incorporation of more comprehensive human data collection, with higher anatomical resolution, could lead to systemic biokinetic model improvement, and ultimately more accurate bioassay predictions.

D. The Expansion of Brain Biokinetics to Biokinetic Model of Aluminum

The current systemic biokinetic model structure for aluminum does not explicitly express brain biokinetic trends. In the interest of monitoring toxicological effects potentially related to chronic aluminum exposures, a brain compartment should be added in future model structure iterations. Specifically long-term brain retention needs to be monitored with concern for aluminum's potential association with Dialysis Dementia, Alzheimer's disease, and other potential neurological issues.[1, 3]

REFERENCES

1. S. Keith, United States. Agency for Toxic Substances and Disease Registry., Syracuse Research Corporation., United States. Environmental Protection Agency., "Toxicological profile for aluminum," (U.S. Dept. of Health and Human Services, Public Health Service, Agency for Toxic Substances and Disease Registry,, [Atlanta, GA], 2008), pp. xx, 310, A-310, B-318, C-316, D-312 p.

2. S. Keith, United States. Agency for Toxic Substances and Disease Registry., United States. Environmental Protection Agency., Syracuse Research Corporation., "Toxicological profile for tungsten," (Agency for Toxic Substances and Disease Registry,, [Atlanta, Ga.], 2005), pp. xix, 163, A-162, B-167, C-165, D-162 p.

3. N. Priest, "The biological behaviour and bioavailability of aluminium in man, with special reference to studies employing aluminium-26 as a tracer: review and study update," Journal of Environmental Monitoring 6, 375-403 (2004).

4. J. Kalinich, C. Emond, T. Dalton, S. Mog, G. Coleman, J. Kordell, A. Miller, D. McClain, "Embedded weapons-grade tungsten alloy shrapnel rapidly induces, metastatic high-grade rhabdomyosarcomas in F344 rats," Environmental Health Perspectives 113, 729-734 (2005).

5. "IMBA Professional Plus Internal Dosimetry Software," (Public Health England, 2013).

6. ICRP, "ICRP Publication 66: Human respiratory tract model for radiological protection," International Commission on Radiological Protection 66(1994).

7. ICRP, "ICRP Publication 30: Limits for intakes of radionuclides by workers," International Commission on Radiological Protection 30(1979).

8. R. Leggett, "A model of the distribution and retention of tungsten in the human body," Science of the Total Environment 206, 147-165 (1997).

9. E. Nolte, E. Beck, C. Winklhofer, C. Steinhausen, "Compartmental model for aluminium biokinetics," Human & Experimental Toxicology 20, 111-117 (2001).

10. C. Steinhausen, G. Kislinger, C. Winklhofer, E. Beck, C. Hohl, E. Nolte, T. Ittel, M. Alvarez-Bruckmann, "Investigation of the aluminium biokinetics in humans: a Al-26 tracer study," Food and Chemical Toxicology 42, 363-371 (2004).

11. D. Taylor, R. Leggett, "A generic biokinetic model for the lanthanide elements," Radiation Protection Dosimetry 79, 351-354 (1998).

12. D. Taylor, R. Leggett, "A generic biokinetic model for predicting the behaviour of the lanthanide elements in the human body. (vol 105, pg 193, 2003)," Radiation Protection Dosimetry 106, 281-281 (2003).

13. R. Leggett, L. Williams, D. Melo, J. Lipsztein, "A physiologically based biokinetic model for cesium in the human body," Science of the Total Environment 317, 235-255 (2003).

14. R. Leggett, "The biokinetics of inorganic cobalt in the human body," Science of the Total Environment 389, 259-269 (2008).

15. R. Leggett, "A biokinetic model for manganese," Science of the Total Environment 409, 4179-4186 (2011).

16. R. Leggett, "The biokinetics of ruthenium in the human body," Radiation Protection Dosimetry 148, 389-402 (2012).

17. ICRP, "ICRP Publication 100: Human alimentary tract model for radiological protection," International Commission on Radiological Protection 100(2006).

18. W. Hinds, Aerosol Technology: properties, behavior, and measurement of airborne particles, 2 ed. (John Wiley & Sons, Inc., New York, 1999).

19. M. Cheng, C. Jenkins, "Production and dynamics of ultrafine and fine particles in contained detonations of aluminium energetics," Journal of Aerosol Science 36, 1-12 (2005).

ACRONYMS

AFRL .....Air Force Research Laboratory
AIBD.....Aluminum-Induced Bone Disease
CMD .....Count Median Particle Diameter
HPA.....Health Protection Agency
HRTM.....Human Respiratory Tract Model
ICRP.....International Commission on Radiological Protection
IEF.....Intake Excretion Fractions
IMBA .....Integrated Modules for Bioassay Analysis
INDOS .....Internal Dose
IRF .....Intake Retention Fractions

DISTRIBUTION LIST
AFRL-RW-EG-TR-2014-016

*Defense Technical Info Center
8725 John J. Kingman Rd Ste 0944
Fort Belvoir VA 22060-6218

AFRL/RWME (6)
AFRL/RWOC-1 (STINFO Office)